Engineering Structures 123 (2016) 451–472

Contents lists available at ScienceDirect

Engineering Structures

journal homepage: www.elsevier.com/locate/engstruct

Full-field measurement with a digital image correlation analysis of a shake table test on a timber-framed structure filled with stones and earth

Y. Sieffert [a,b,*], F. Vieux-Champagne [a,b,c], S. Grange [a,b], P. Garnier [c], J.C. Duccini [d], L. Daudeville [a,b]

[a] Univ. Grenoble Alpes, 3SR, F-38000 Grenoble, France
[b] CNRS, 3SR, F-38000 Grenoble, France
[c] CRAterre, AE&CC Research Unit, National School of Architecture of Grenoble, France
[d] FCBA, French Technological Institute for Forestry, Cellulose, Timber Construction and Furniture, Bordeaux, France

ARTICLE INFO

Article history:
Received 10 July 2015
Revised 19 February 2016
Accepted 7 June 2016

Keywords:
Shake table
Digital image correlation
Seismic tests
Earthquake
Haiti
Traditional houses
Rural houses
Wood-frame structure
Stonework masonry
Earth mortar

ABSTRACT

This paper aims at presenting a digital correlation technique to capture the full-field displacement thanks to a high-speed camera of a full scale structure tested on a shaking table. The challenges are both the measurements at a full scale to visualize damages versus the resolution of pictures and the dynamical loading that requires a large number of pictures. The final goal is a better understanding of the seismic behavior of timber-framed structures with infill to help at modeling such structures and predicting their seismic vulnerability. For this purpose, results of shake table tests carried out on a full-scale one-story timber-framed house filled with stones bonded by an earth based mortar are presented and discussed. DIC full-field measurements allow deriving displacements and accelerations on shear walls as well as lateral forces applied on them. The experimental results presented herein allow analyzing the influence of bracing and might be used to propose optimized aseismic constructions based on cheap technological solutions. These results demonstrate the seismic-resistant behavior of timber-framed structures with infill and constitute a key issue for the promotion of such constructions in developing countries.

1. Introduction

From a worldwide perspective, the construction industry is arguably one of the most resource-intensive and environmentally damaging. This sector accounts for 40% of the total flow of raw materials into the global economy each year [11]. Given the coming shortage of raw materials (sand, cement, metals, [24,8]) coupled with the need to promote sustainable and virtuous development for the planet particularly within the building sector, bio-based and completely reversible materials must be developed. Timber-framed structures filled with earth and other locally available materials might constitute one response to the challenges associated with human settlement and construction sector challenges. Moreover, this type of structure is found throughout the world and heavily present in seismic prone areas [28] by offering the double advantage of meeting the population's local capacity constraints (economic and available materials) and featuring an intrinsically seismic-resistant behavior. These kinds of structures unfortunately have been overlooked by locals and decision-makers due to a lack of knowledge of their potential behavior and a lack of building codes and standards for their proper design.

In many countries across the world, reinforced concrete structures have nearly unanimously replaced the vernacular architectural style within a single generation. This rapid transition may be explained by the fact that reinforced concrete buildings are typically associated with modernity, whereas more traditional construction is perceived as suboptimal and old-fashioned [13]. However, following the latest earthquakes in many developing nations, a large number of poorly reinforced concrete buildings collapsed, leading to widespread destruction and loss of life, while well-maintained traditional vernacular neighboring structures survived in sustaining just slight damage [14]. Poor design,

* Corresponding author at: Univ. Grenoble Alpes, 3SR, F-38000 Grenoble, France.
E-mail addresses: yannick.sieffert@3sr-grenoble.fr (Y. Sieffert), florent.vieux-champagne@3sr-grenoble.fr (F. Vieux-Champagne), stephane.grange@3sr-grenoble.fr (S. Grange), craterre.pgarnier@club-internet.fr (P. Garnier), jean-charles.duccini@fcba.fr (J.C. Duccini), laurent.daudeville@3sr-grenoble.fr (L. Daudeville).

http://dx.doi.org/10.1016/j.engstruct.2016.06.009
0141-0296/

(a) Urban project in Port-au-Prince (Entrepreneurs du Monde)

(b) Rural project in Terre rouge, 10th section of Petit-Goâve (Concert-Action and Misereor project, photo by Elsa Cauderay)

(c) School two-storey project in Grand Boulage, (Entrepreneurs du Monde)

Fig. 1. Buildings completed for reconstruction projects.

Fig. 2. The house on the shake table.

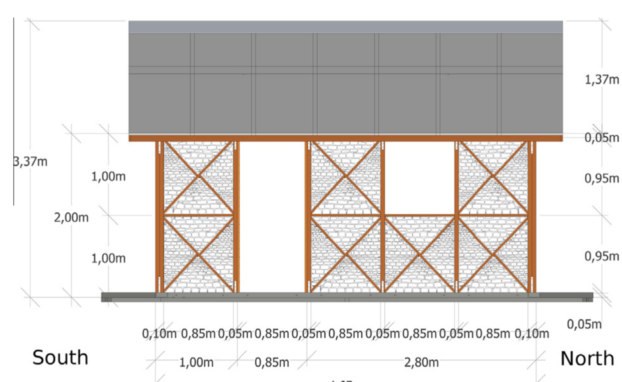

Fig. 3. Dimensions of the wall recorded by camera (East shear wall).

inadequate construction techniques and cost savings would be reasonable explanations behind many reinforced concrete failures [5].

For a safer and greener planet, infilling timber-framed structures with local materials, wherever relevant, should be promoted to move towards more sustainable development and to cease wasting the precious resources that led to the domination of reinforced concrete structures, even when conditions are not absolutely dire. Recently, a number of research projects have been conducted to further the state of knowledge on seismic-resistant behavior, in drawing comparisons with traditional timber-framed structures using infill (e.g. at the wall scale: [17,20,2,3,1,7,28]).

Table 1
Shake table characteristics.

Dimensions	6×6	m^2
Weight	6	tons
Payload	10	tons
Max. dis.	± 0.125	m
Max. vel.	0.75	m/s
Max. acc.	4	g
Frequency range	0–30	Hz
Overturning moment capacity	250	kN m

The mains conclusions of these studies are: (1) the infill material contributes to the ultimate bearing capacity and ductility increases thanks to the confining effect of the timber frame and (2) most of damage phenomena are concentrated in connections. All shear tests involved in this campaign have been based on quasi-static loadings.

The aim of this paper is to present the results of actual seismic tests performed on a full-scale house at a shake table facility. The house studied herein is a timbered masonry structure adapted from Haitian heritage, called "*Kay peyi*". This type of structure has already been built in Haiti as part of various local reconstruction projects (i.e. Misereor, SC/CF projects in collaboration with the CRAterre Laboratory and local partners, including the Haitian NGO "GADRU", Entrepreneurs du Monde). The purpose here is to deliver a scientific assessment of structural implementation by employing an effective combination of a high-speed camera and the digital image correlation (DIC) technique.

Structural monitoring in the field of Civil Engineering for dynamic loadings is generally performed using contact systems, such as displacement or acceleration transducers. Despite many advances in these systems over recent years, non-contact measurement systems have also been developed in parallel, and abundant references are now available (see [21] for references and comments on various technologies: laser, radar, GPS, video and photography). For the DIC technique, given the structural engineering scale, measurements remain local and targets are associated in order to track dynamic displacements [10,25,21]. Full-field displacements have been used however to detect the structural damage of a beam element on a dynamic test in Shih and Sung [23].

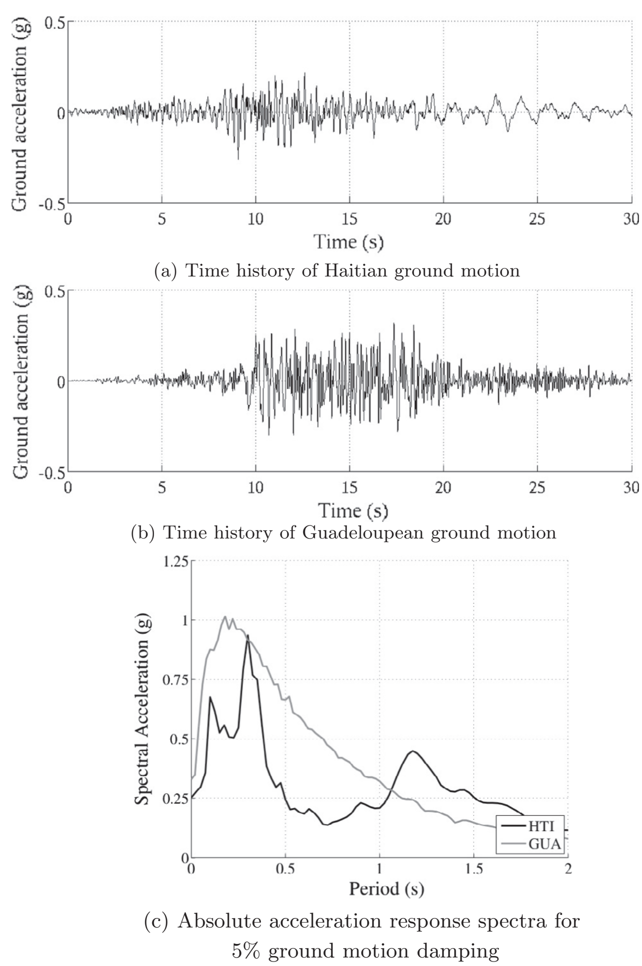

(a) Time history of Haitian ground motion

(b) Time history of Guadeloupean ground motion

(c) Absolute acceleration response spectra for 5% ground motion damping

Fig. 4. Time and frequency content of the Haitian and Guadeloupean ground motions.

Table 2
Seismic test sequence.

Ground motion	Amplitude scaling factor	Scaled max. displ. (mm)	Scaled max. velocity (m/s)	Scaled PGA (g)
Haiti 100%	1	35.7	0.158	0.27
Haiti 200%	2	71.4	0.316	0.54
Haiti 300%	3	107.1	0.474	0.77
	Reparation operation			
Guadeloupe 100%	1	30.9	0.168	0.32
	Reparation operation			
Guadeloupe 390%	3.9	117.3	0.637	1.26

In a previous paper, Vieux-Champagne et al. [27] presented the principal results of the Haitian house in the shake table test, with a focus on measurements using local transducers: Linear Variable Differential Transformer (LVDT), Draw Wire Displacement Sensor (DWDS), and accelerometer. The findings of a DIC analysis were also provided as a means of validating the method applied at this scale. For this purpose, only local results obtained by DIC were displayed and compared with those from a local sensor. The aim of the present paper is to take the analysis one step further by introducing the full-field displacement. To the best of the authors' knowledge, this effort marks the first time that a full-field measurement has been accomplished in meeting the double challenge of: working at the structural (single house) scale, and using a shake table to apply loading. This field measurement yields a new understanding of the seismic-resistant behavior of timber-framed structures. In light of these experimental results, the bracing effect is achieved through use of various ground motion signals.

The body of this article will be divided into five sections: the first will briefly present the shake table test program. The second will describe the DIC set-up (camera, lighting, speckle pattern, software and output visualization), while the third section will provide a validation of the adopted method. Section 4 will expose the results obtained during the field measurement. Moreover, insight will be shared into both the debonding between bracing and infill and the global hysteretic responses of the shear wall. Lastly, the effects of bracing will be discussed in the context of high-energy ground motion signals.

2. Experimental set-up

This part presents the experimental set-up to perform the seismic test on the timber framed structure containing infill. First, the

Table 3
Technical characteristics of system components.

Video camera	Technical characteristics
Brand/model	Phantom v641
Maximum resolution	2560 × 1600 HD
Frequency at maximum resolution	1450 fps
Memory	8 up to 32 Gigabits
Added memory	128–512 Gigabits phantom CineMag
Pixel size	10 μm
Sensor	CMOS
Color	monochrome
Output	Gigabit ethernet
Lensing	F-mount, C-mount, PL-mount
Triggering	hardware trigger BNC
Software	CineMag to CineStation®
Dimensions	29.2 × 14 × 12.7 cm
Weight	5.33 kg

Table 4
Configuration selected.

Video camera	Technical characteristics
Brand/model	Phantom v641
Resolution	2560 × 1600 HD
Frequency	150 fps
Added memory	128 Gigabits phantom CineMag
Time recorded	50 s
Triggering	hardware trigger BNC with other measurement devices (lvdt and accelerometers)
Lensing	Nikkor Ai-S 28 mm f/2
Distance from the wall	6.1 m
Horizontal field of view	5.4 m
Resolution	2.16 mm/px

Table 5
Lighting configuration selected.

Lighting	Technical characteristics
Brand/model	4 K alpha version
Power	4000 W
Frequency ballast	1000 Hz
Option	shallow alpha
lamp	Open-Eyes HMI, ceramic G38 socket
Dimensions	53 × 58 × 36 cm
Weight	20.4 kg
Distance from the wall	6.5 m

building design is depicted, then the shake table and the test program are described. Lastly the main characteristics of the ground motions played are given and the location measurement devices (DWDS, LVDT and camera) are shown.

2.1. Building configuration

The house studied herein is a wood structure with infill. This type of construction is common in many countries (including France, Germany, Italy, Pakistan, India and Haiti (see [12,16,6]), in recognition of the ability in most cases to use natural materials available on-site). This solution therefore is environmentally friendly (which is a key concern in developed countries) while offering simpler building conditions and lower costs (major considerations in emerging countries).

The selected house is prevalent in Haitian timber-framed reconstruction programs initiated after the 2010 earthquake; it provides an enhancement over traditional buildings by improving the connection of the timber structure with both the basement and foundation, and by introducing bracing via San Andrew's crosses (X-cross) filled with natural stones and bonded by earth mortar using sisal. Fig. 1 presents the set of structures used in numerous reconstruction projects (in rural as well as urban settings). The proposed research concerns the first stage of the reconstruction program that is focused on rural and peri-urban housing which typically consists in one-story houses. Based on presented research results, two-story buildings were designed and built later (e.g. a school, Fig. 1c).

The X-crosses simplify the structural filling step and moreover improve safety in the event of falling stones thanks to smaller-sized infill components, although at some financial cost since wood pieces are not easy to procure by the local population. The bracing is composed of a single continuous diagonal and another diagonal divided into two parts; the bracing configuration is bonded using 70-mm long wooden nails, and the non-continuous diagonals are purposely misaligned in order to simplify nailing. These techniques serve to facilitate construction and avoid weakening the wood, as opposed to an edge half-lap joint located at the center of each diagonal.

Various connections have been implemented to build the structure described previously in Vieux-Champagne et al. [28]: type 1 is a steel-wood nailed joint; type 2 is the joint between the middle post, the bracings and the nogging; while the ligature wire provides the connection between roof and wall.

The house built for the shake table test covers a footprint of $4.65 \times 4.65\ m^2$; it is 3.37 m high (at the ridge) and symmetrical with respect to the N–S axis (i.e. the loading direction, see Figs. 2 and 3). Three weeks were needed to build the house on the shake table in deploying a multidisciplinary team of 8 architects and 3 civil engineers.

The shear walls have six vertical posts, with a window and door respectively between posts 2–3 and 4–5 in the N–S direction (Figs. 3 and 10). The transverse walls are identical, with six vertical posts as well and one window located between posts 3 and 4. According to a preliminary numerical study, the specimen was placed on the shake table in order to load its weaker direction; it was anchored into steel beams, which themselves had been bolted onto the table. The dimension of each wall equals 4.65 m by

Fig. 5. Overview of system components (shear wall tracked, lighting and camera positions).

Fig. 6. Projected paint droplets.

Fig. 7. Overview of speckle patterns.

2.00 m, which corresponds to 9.3 m^2. Only the East shear wall shown in Fig. 3 was filmed by cameras.

2.2. Shake table test program

These dynamic tests were performed on the uniaxial earthquake simulation facility in the Mechanical Laboratory at the French FCBA Institute (in Bordeaux). The shake table is composed of a $6 \times 6\ m^2$ aluminum platform moved by a 250 kN servo-hydraulic actuator. Table 1 lists the various shake table characteristics.

2.3. Simulated ground motions

For purposes of this research, a strong ground motion had to be simulated since no seismological recording of the January 12th, 2010 earthquake was ever available. It corresponds to a Mw 6.8 earthquake occurring 34 km west of Port-au-Prince. A second motion was simulated by fitting an empirical spectrum characteristic of seismic activity in the French West Indies. These two signals featured the same approximate peak ground acceleration, near 0.30 g. Fig. 4 summarizes these results in terms of an elastic response spectrum and the corresponding time history in acceleration.

As indicated above, the tests carried out sought to demonstrate the safe behavior of the structure under seismic loading. The simulated signal representative of Haiti's January 2010 earthquake was first selected in order to determine the seismic-resistant behavior associated with this particular type of construction. This simulated signal was denoted "Haiti 100%". Next, the signal was increased to an extent matching the shake table capacity (Table 2) so as to analyze the nonlinear structural behavior (i.e. Haiti 200% and Haiti 300%). After these 3 loadings, the apparent damage of the house seemed to be very low with all damage ascribed to deformation of the transverse walls and roof structure. A number of repairs were then performed (see Section 3). After this reparation operation, it was impossible to still increase the same signal because "Haiti 300%" has led to a shake table displacement close to its maximum capacity. The second signal, i.e. the so-called "Guadeloupe 100%" was selected because of a PGA close to the one of "Haiti 100%" and an extremely good fit with the shake table displacement capacity at a 3.9 scaling factor (i.e. "Guadeloupe 390%"). Moreover this signal corresponds to a scenario that can be found in the French West Indies islands (Antilles) close to Haiti.

"Guadeloupe 390%" gives a maximum overturning moment solicitation around 80 kN m which is 3 times less than the overturning moment capacity of the shake table.

Table 6
Pixel tracking descriptions.

Part	For one cell (pixel)
Intermediate beam	15
Andrew's cross	40
Infilled materials	484
Part	**For the wall (pixel)**
Timber-framed	580
Infilled materials	3388
Shake table	1

2.4. Experimental imaging set-up

The measured displacement results using DIC are influenced by: the measurement system, lighting conditions, and speckle pattern. These three primary elements will be discussed below.

2.4.1. Camera

A high-speed camera with a high resolution, i.e. the Phantom v641, was used to track motion. The technical characteristics of this camera are given in Table 3. This maximum resolution (2560×1600) is necessary to obtain the most accurate DIC analysis. At this resolution, each pixel represents 2.16 mm on the wall. The frame rate was correlated with the test duration to respect the memory storage capacity constraints. The seismic signals used in this study are 30 s longer (Fig. 4). For practical reasons, a 50-s signal has been recorded. Thanks to an additional 128 gigabytes (GB) of memory, a 150-frame per second rate could be used. The file size of a movie for one signal is 40 Gigabites. After extraction,

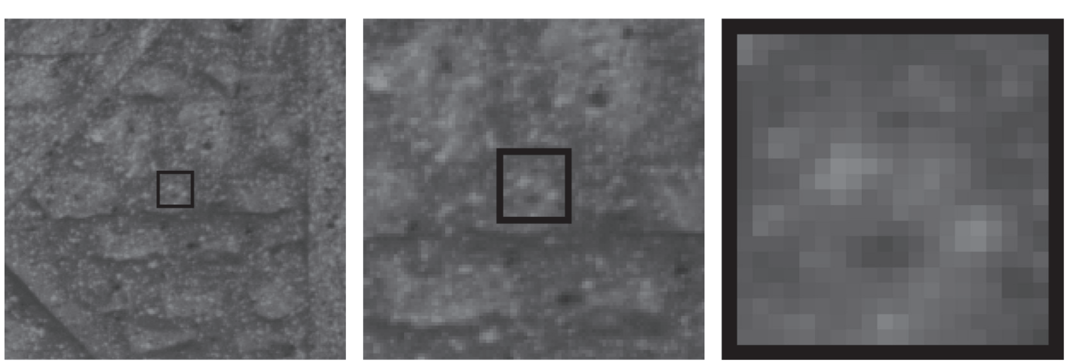

(a) image size: 200×200 pixels (b) image size: $100 \times$ pixels (c) image size: 20×20 pixels

Fig. 8. Gray scale of one speckle pattern with a 20×20 subset at different zoom levels.

each earthquake leads to 7500 images. The image file size is 8.2 Megabites in.tif format. Table 4 shows the configuration set-up employed for this study.

The camera measurement system was synchronized with a conventional contact measurement apparatus: Draw Wire Displacement Sensor (DWDS), Linear Variable Differential Transformer (LVDT), and accelerometer. Each of these apparatuses was connected to a BNC cable. For simultaneous acquisitions, BNC signal provided by the acquisition of the conventional contact is used to trigger the recording action of the camera and conventional contact measurement apparatus. A constant delay time of 0.6367 s was observed between the camera and the contact measurements, most likely as a result of the intrinsic time required to open the photocathode gate and start recording.

2.4.2. Lighting

Measurement precision with a high-speed camera depends in large part on image brightness, hence background lighting is required. In this study, two challenges are raised regarding lighting: (1) the same light intensity is required along the wall and (2) the lighting must not create a shadow due to the wall's thickness and roughness texture. The lighting must also be as diffuse and far from the wall as possible. The use of several lighting sources is indeed a solution, yet one difficult to calibrate. A powerful lighting source (4000 W, 4 K alpha version) positioned 6.5 m away from the wall was the preferred solution (Fig. 5). Table 5 lists the technical characteristics of this 4 K alpha version. A high-frequency ballast was also installed to protect against a flicker of the camera frequency acquisition. In addition, a shallow alpha was inserted to create a spatial lighting effect.

2.4.3. The speckle pattern

According to the DIC technique, a pixel is tracked from one image to another using a pixel signature defined by a gray value. Since the gray value of a pixel could not be unique, a subset containing neighboring pixels were associated at the pixel signature. To obtain accurate measurements, this subset required a speckle pattern to distinctly demonstrate different gray scale distribution characteristics [19]. This step could not be completed solely with the natural specimen surface, which is a repeated combination of earth, timber and stone texture. A random painted speckle pattern then had to be added. Pan et al. [19] and Lecompte et al. [15] showed that the speckle size in a given speckle pattern, combined with the size of the subset, exerted an influence on the displacement measurement accuracy. A distributed speckle pattern, in terms of radius, is more suitable than the smallest possible speckles. Hua et al. [9] indicated that speckle patterns should display a speckle from 2 to 4 pixels and a high density. The speckle pattern is typically produced with a can of spray paint. This technique however cannot be used with the test's wall dimensions and camera resolution since the dots would be too small. Acrylic paint cans and brushes were thus used in conjunction with a special technique of droplets projected by dynamic shock created when the wrist movement was suddenly stopped (Fig. 6). This technique ensures obtaining both a random dot size (between 1 and 10 mm) and a satisfactory dot density within a relatively short time. With the optimum subset of this test (see Section 2.4.4), the speckle dimension is close to 1–6 pixels (Fig. 8). Three paint colors were used to create the gray scale: black, gray, and white (Fig. 7).

2.4.4. Tracker

The DIC software named "Tracker" used for this paper [4,22] had initially been developed for granular materials. In the presence of rigid motion, Tracker is a robust parallelized code with a sub-pixel resolution obtained by a bilinear interpolation function of

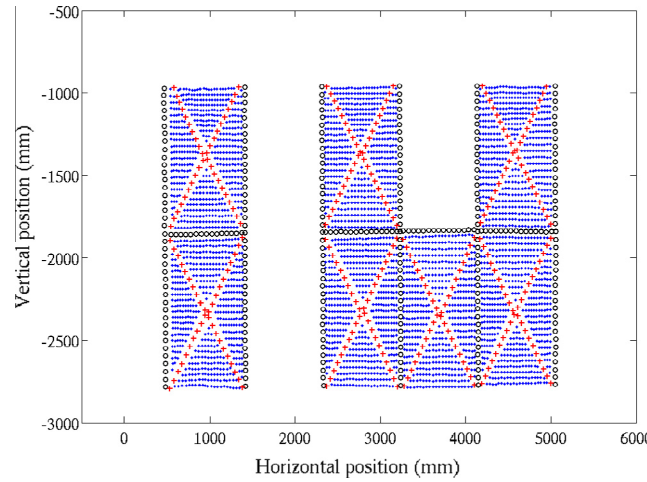

Fig. 9. Measurement field visualization.

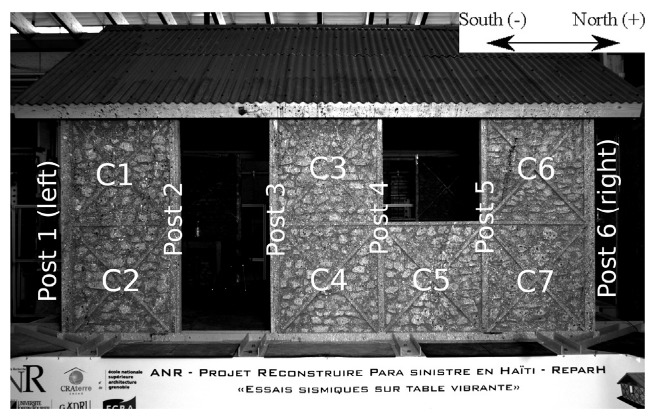

Fig. 10. Name of the square parts.

gray levels covering the subset tracked over all images. The sub-pixel resolution is based on the Zero-mean Normalized Cross-Correlation (ZNCC) criterion [18]. The estimate is independent of differences in brightness and contrast due to the normalization with respect to mean and standard deviation.

The greater relative displacement on the wall is approx. 4 cm (Tables 8 and 9), which substantiated the hypothesis of rigid motion as regards the wall's dimensions (i.e. whereby the pattern of a given subset remains unchanged after the transformation). This hypothesis proves to be beneficial since the tracking is not performed between successive photographs, which in turn leads to an accumulation of digital truncation errors in the sequential processing of images. Instead, the tracking is directly carried out between the first current photographs.

As highlighted above, the subset size and speckle pattern are correlated. An optimal subset (i.e. rectangular with 20 × 20 pixels) is formed according to two observable data components: shake table displacement measured by the LVDT, and the Tracker code's capacity to follow every part of the wall independently (timber-framed structure, Andrew's crosses, earth and stone). The timber-framed structure with Andrew's crosses is tracked with a linear mesh along the local neutral axis of each element. To track the infill material, a special precaution is introduced to associate, at each pixel, a subset pixel with just infill material inside (i.e. no wood) to avoid difficulties when seeking this subset if debonding appears at the interface with the Andrew's crosses.

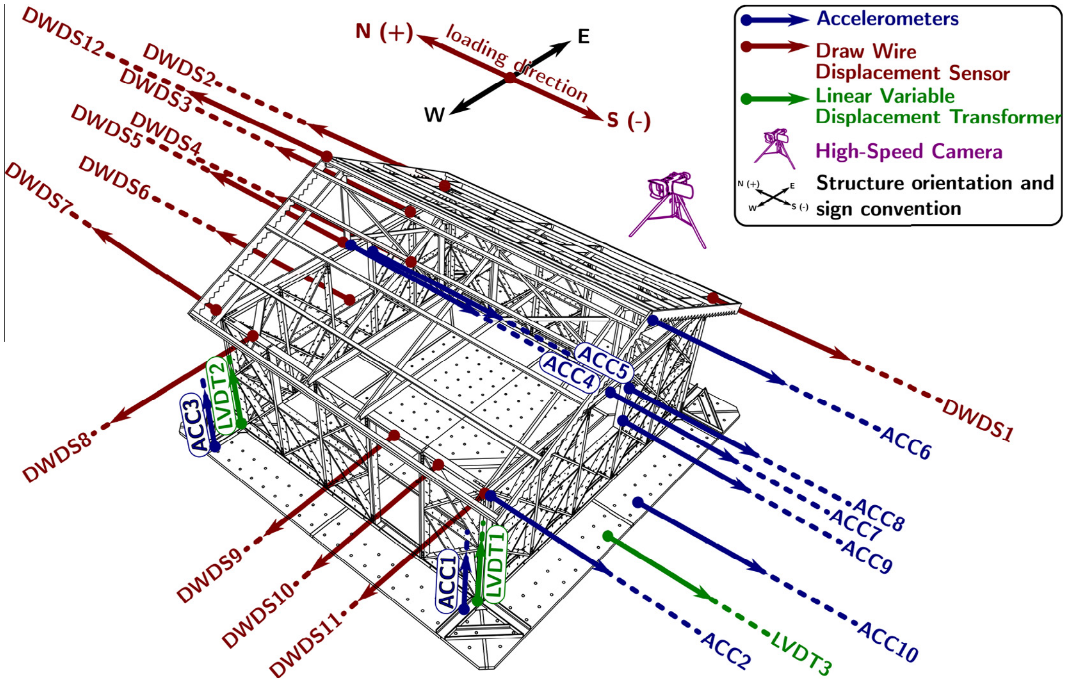

Fig. 11. Measurement device position.

(a) Haiti 200%: Connection – Location: South transv. wall

(b) Haiti 300%: Connection – Location: South transv. wall

(c) Guadeloupe 390%: Connection – Location: South transv. wall

(d) Guadeloupe 390%: Overview of damage

Fig. 12. Main damages observed in the south transverse wall (most damaged) – debonding of infill and steel strip deformation.

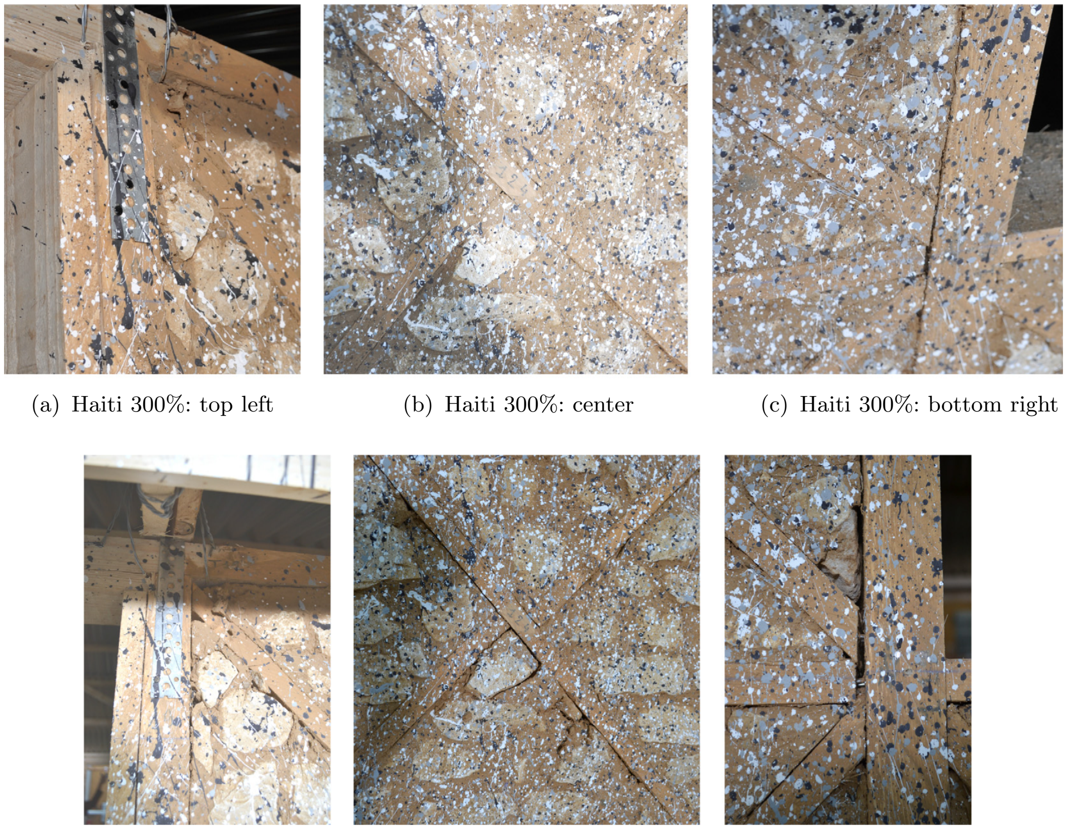

(a) Haiti 300%: top left (b) Haiti 300%: center (c) Haiti 300%: bottom right

(d) Guadeloupe 390%: top left (e) Guadeloupe 390%: center (f) Guadeloupe 390%: bottom right

Fig. 13. Damage observed in the shear wall – mainly debonding of infill.

2.4.5. Output visualization, nomenclature and sign convention

Nearly 4000 pixels were tracked in order to describe the global response of the test wall (Table 6). Three pixels on the shake table were used at the beginning of this study; they have yielded exactly the same displacement, thus making it possible to deal with one pixel. Two distinct representations have been used in this paper for the full-field measurement, with one being the actual deformation drawn with the circle or cross (Fig. 9) and the other containing a vector drawing the displacement between the initial configuration and the deformation configuration. To aid with the visualization, an amplification factor is always introduced (as indicated in each figure). The black color depicts the beam or post, while red represents the Andrew's crosses and blue the infill material. Let's note that the infill material has not been shown with the vector visualization so as not to overload the figures.

The sign convention is displayed in Fig. 10. When a displacement lies in the right direction (north) it has a positive value, and the left direction (south) is depicted by a negative value.

2.5. Contact devices set-up

In addition to high-speed camera and the DIC technique, contact measurement devices were used according to the layout shown in Fig. 11. Displacements were measured thanks to DWDS and LVDT transducers while accelerations were recorded with accelerometers. As the aim of this paper is not to take advantage of all the results given by these local transducers, but to demonstrate the feasibility of tracking a full-field displacement using a high-speed camera and digital image correlation (DIC) technology, only this latter technique is explained and detailed. Only the shake table displacement (LVDT3) and acceleration (ACC10) measurements are provided hereafter for a comparison with displacements and accelerations obtained with recorded camera images. The shake table displacement is measured with the integrated LVDT of the actuator (RDP with a range of ± 150 mm).

3. Observed damage and reparation

This section describes the main damage observed during the seismic test program with a specific focus on the East shear filmed by camera. The main observed damage is depicted in Fig. 12. Steel strips used in connections exhibited significant plastic deformations and nails were deformed and partially pulled out of wood members. Such damage phenomena contribute to a high ductility of the structure. Despite some connection pull-outs in the roof structure and local infill debonding, most part of the visible damage is located in the transverse wall that was submitted to significant out-of-plane deformation. Nevertheless, such damage did not affect the structural stability. The transverse wall infill started debonding and cracking during the "Haiti 200%" seismic test and was pulled out during the "Guadeloupe 390%". During the "Haiti 100%" test, no damage was observed. After "Haiti 300%", a repairing operation was performed. It mainly consisted in driving again partially pulled-out nails. During "Guadeloupe 100%" test, few additional damage occurred.

Before "Guadeloupe 390%" earthquake no damage has been observed on shear walls. To highlight the damage observed, Fig. 13 shows the same part of the wall after "Haiti 300%" and "Guadeloupe 390%". At this stage, wood and infill triangles started debonding. Since this damage is not easily visible, especially during

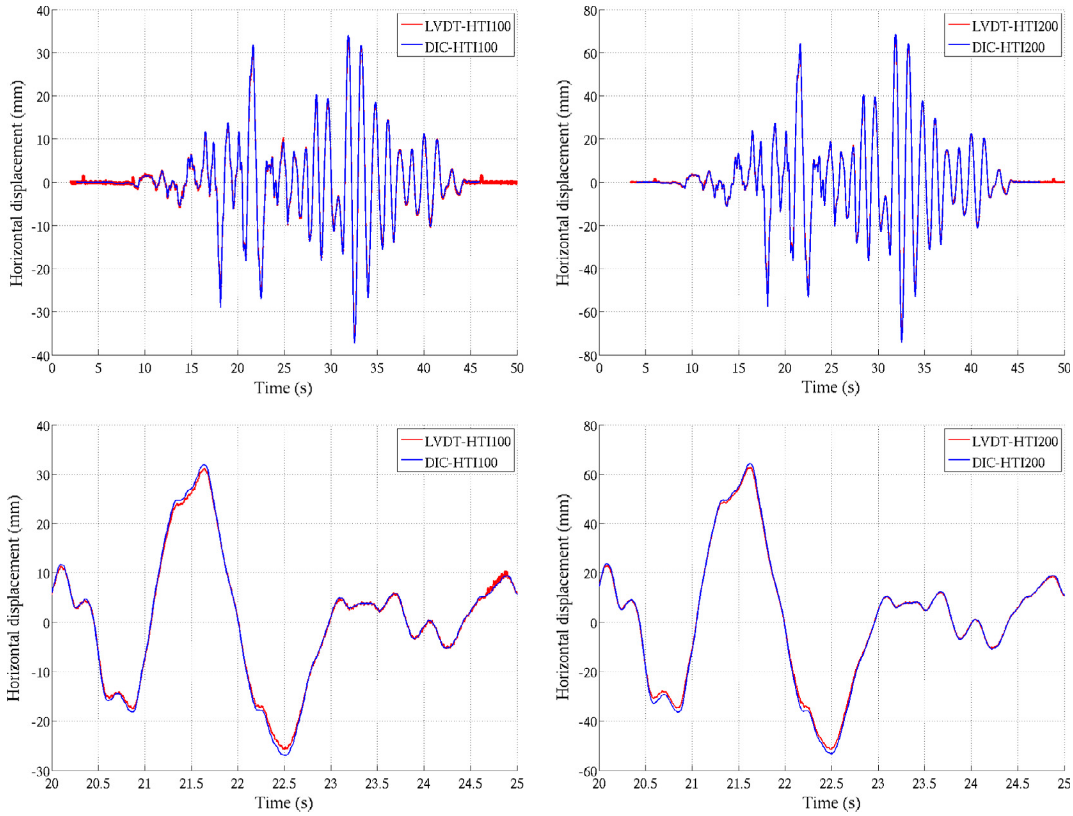

(a) Haiti 100%

(b) Haiti 200%

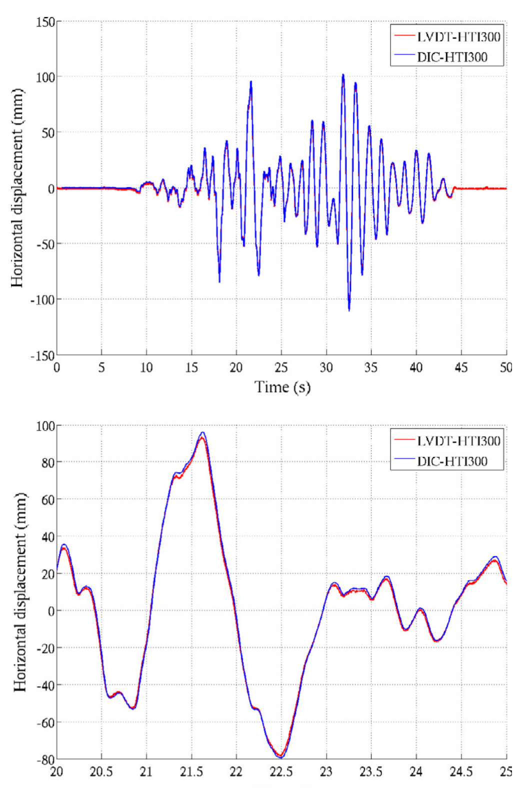

(c) Haiti 300%

Fig. 14. Haiti – comparison between DIC and LVDT for shake table displacement (all signals and a close-up near the peaks).

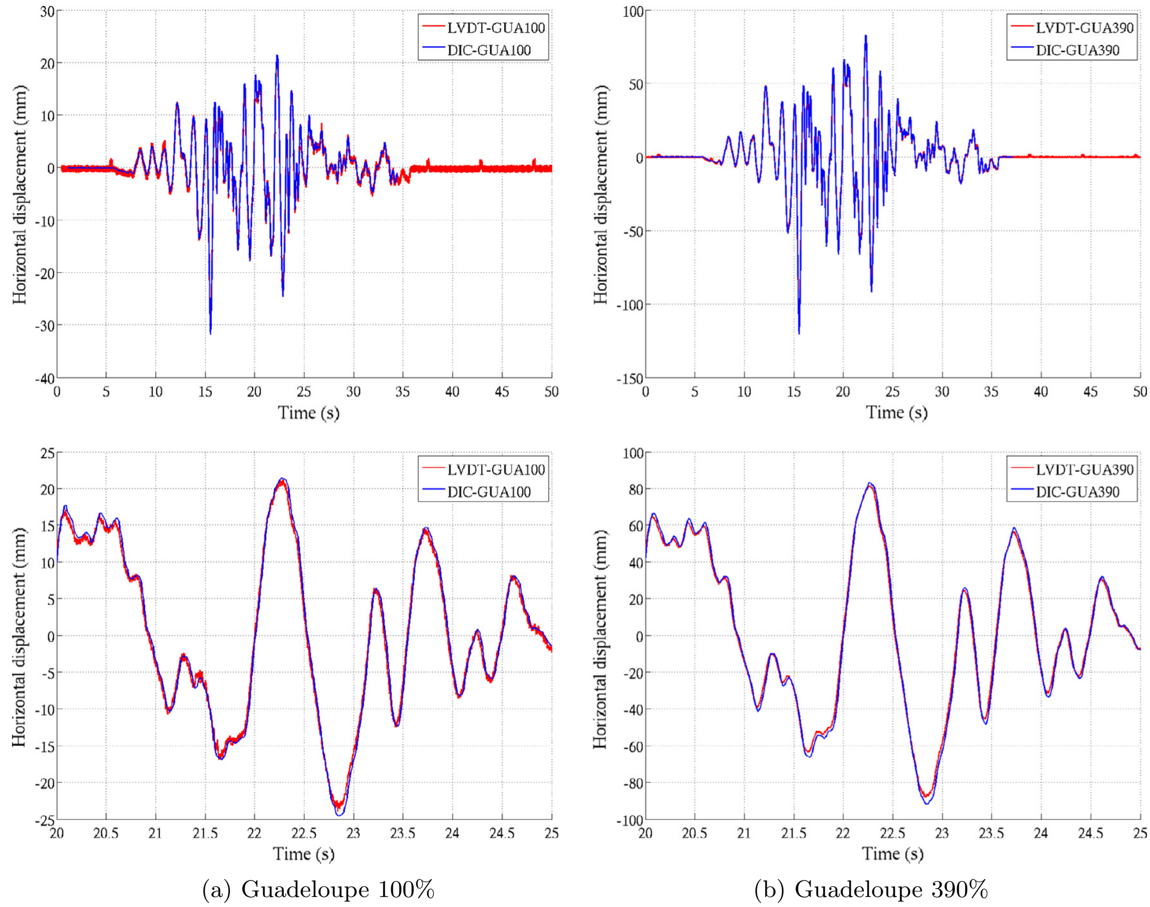

Fig. 15. Guadeloupe – comparison between DIC and LVDT for shake table displacement (all signals and a close-up near the peak).

Table 7
Maximum difference between DIC and LVDT methods for the shake table.

Earthquake	Haiti 100%	Haiti 200%	Haiti 300%	Guadeloupe 100%	Guadeloupe 390%
LVDT displacement (mm) for the maximum difference	−25.85	−51.72	93.10	−23.74	−87.47
DIC displacement (mm) for the maximum difference	−26.98	−53.29	96.01	−24.58	−91.83
Difference (%)	4.3	3.0	3.1	3.5	5.0

Table 8
Maximum positive U_x displacement.

Earthquake	Position	Image	Time (s)	Displacement (mm)
Haiti 100%	Left post	2314	18.08	1.72
Haiti 100%	Right post	2668	20.44	1.67
Haiti 200%	Left post	2508	20.75	6.19
Haiti 200%	Right post	2508	20.75	6.20
Haiti 300%	Left post	2978	20.49	12.51
Haiti 300%	Right post	2978	20.49	12.02
Guadeloupe 100%	Left post	3337	23.37	4.12
Guadeloupe 100%	Right post	3383	23.68	5.36
Guadeloupe 390%	Left post	3470	23.77	33.70
Guadeloupe 390%	Right post	3468	23.76	36.41

Table 9
Maximum negative U_x displacement.

Earthquake	Position	Image	Time (s)	Displacement (mm)
Haiti 100%	Left post	2643	21.70	−2.15
Haiti 100%	Right post	2643	20.26	−1.60
Haiti 200%	Left post	2533	20.92	−3.75
Haiti 200%	Right post	3186	21.88	−5.74
Haiti 300%	Left post	3061	21.04	−10.28
Haiti 300%	Right post	3062	21.05	−6.54
Guadeloupe 100%	Left post	3355	23.49	−6.79
Guadeloupe 100%	Right post	3356	23.50	−4.86
Guadeloupe 390%	Left post	3441	23.58	−37.67
Guadeloupe 390%	Right post	3439	23.56	−30.07

seismic test, DIC measurements appear relevant for the analysis of the complex cyclic behavior of the wall.

Between "Haiti 300%" and "Guadeloupe 100%", the structure has been fixed in the following way: hammering of pulled out nails, tightening the loosened ligature wires, and putting back in place the roof structure bracing. After "Guadeloupe 100%", since observed damage was only localized on the bracing of the roof structure, only this part was fixed. The infill material, the timber framed structure and the Andrew's crosses have never been fixed.

4. Validation by means of shake table displacement (DIC/LVDT)

As explained above, the wall dimension (greater than 9 m^2) challenges the accuracy of DIC results due to both the lower relative displacement of the structure (between 1 mm and 40 mm) and the camera resolution (2.16 mm/pixel and 0.216 mm/sub-pixel, respectively). Figs. 14 and 15 show a perfect acquaintance for a seismic loading with both high and low energy (high and low shake table displacement and hence structural response). The highest differences between LVDT and DIC are presented in Table 7. These differences are less than 5%. Let's also note that the LVDT signal is noisier than that obtained using the DIC technique.

5. Results

The results of this investigation are presented in the three following subsections: "field displacements", "debonding between infill material and Andrew's crosses", and "acceleration and force".

5.1. Field displacements

This section constitutes the heart of the paper: with 3969 pixels, the entire wall is tracked all along the earthquake signals.

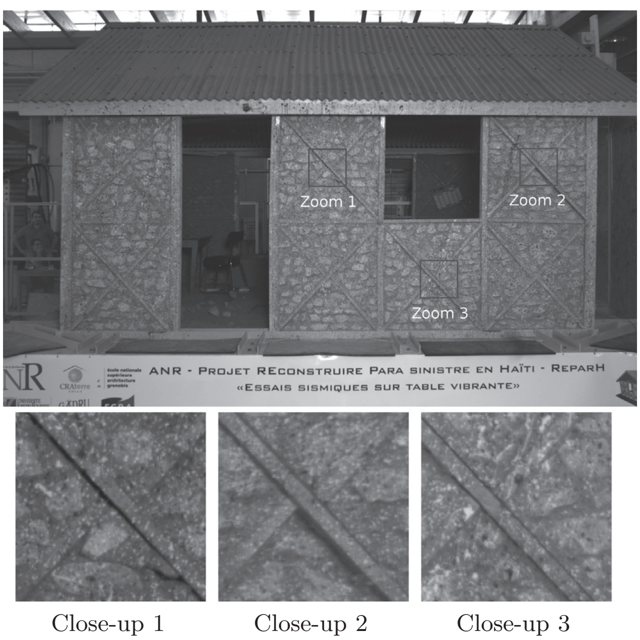

Fig. 16. "Guadeloupe 390%" image with DIC(i) = 3468.

The maximum relative displacements in the x (horizontal) direction are applied and always found on the top left or top right post (Fig. 10). Since the maximum displacements are recorded in either the positive or negative direction, two tables are presented. Table 8 summarizes the maximum displacements in the positive direction, while Table 9 contains the maximum negative displacements. The y (vertical) direction has not been shown given that its displacements are smaller, but it is still worth noting that DIC yields displacements in both the x and y directions, which would be impossible with DWDS or LVDT.

The extreme displacements reveal a similar behavior of the shear wall in both directions; moreover, they remain uncorrelated linearly with the increasing displacement of earthquake signals. A nonlinear behavior can be brought out by comparing the response of the structure under seismic signals "Haiti 100%" and "Haiti 300%". As these two signals exhibit exactly the same frequency contents, they excite an elastic linear structure with the same modal shapes that make possible the comparison of maximum top wall displacements. As the ratio of the ground motion amplitudes between "Haiti 100%" and "Haiti 300%" (3) is lower than the ratio of the maximal top wall displacements (7.3), a nonlinear behavior of the structure can be highlighted; it is especially due to damage. Since nothing is visible on the wall with the naked eye, an investigation has to be conducted in order to understand why the displacement is amplified and where damage occurs. This step will be carried out in the following section.

Another comment worth noting is the non-concomitance of the extreme wall displacements with extreme displacements of the shake table, in association with a large acceleration (i.e. high energy) obtained in the positive direction for Haiti at 21.6 s and for Guadeloupe at 22.3 s. This condition is in fact due to the free vibration of the structure whenever a maximum relative displacement is recorded on the wall in one direction, as the shake table may already be moving in the other direction.

In the following discussion, a representation of the full-field relative displacements of the shear wall will be provided for all earthquake signals studied. This representation is generated by tracking 3969 pixels. For a displacement considered as positive, a visualization is triggered when the maximum relative displacement on the top right post has been reached. With an identical method, once the displacements have been considered as negative, visualization takes place at the time of maximum relative displacement on the top left post. The advantage of the DIC technique is to expose, with the assistance of an amplification factor, the opening in infill material and the flexural behavior of both the timber elements and the

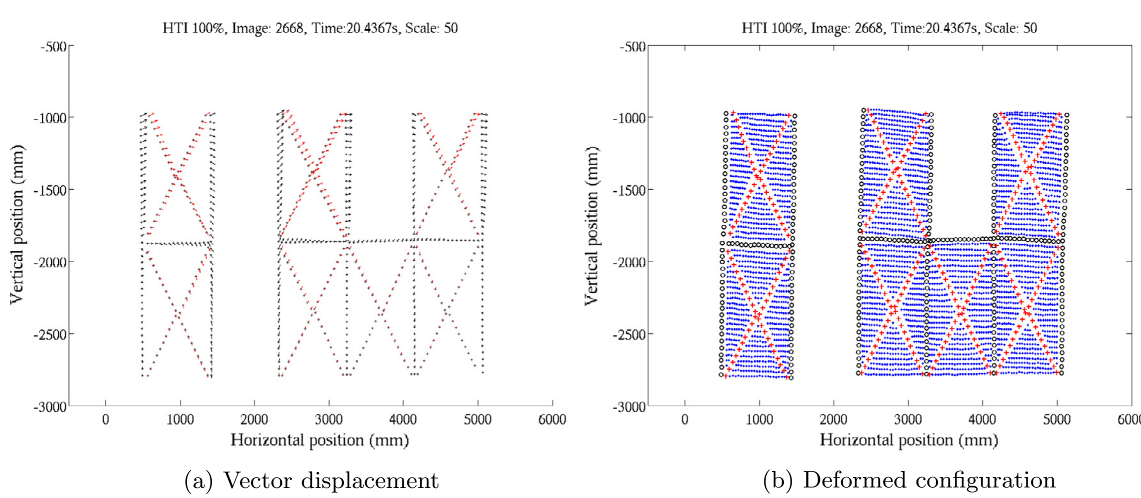

Fig. 17. "Haiti 100%" in the positive direction.

entire timber frame. These observations are practically impossible to record with the naked eye, as illustrated in Fig. 16 for "Guadeloupe 390%".

Figs. 17, 18, 23 and 24 show that the pixels are almost all correctly tracked. For this level of earthquake, the maximum relative displacement is extremely small (close to the pixel definition).

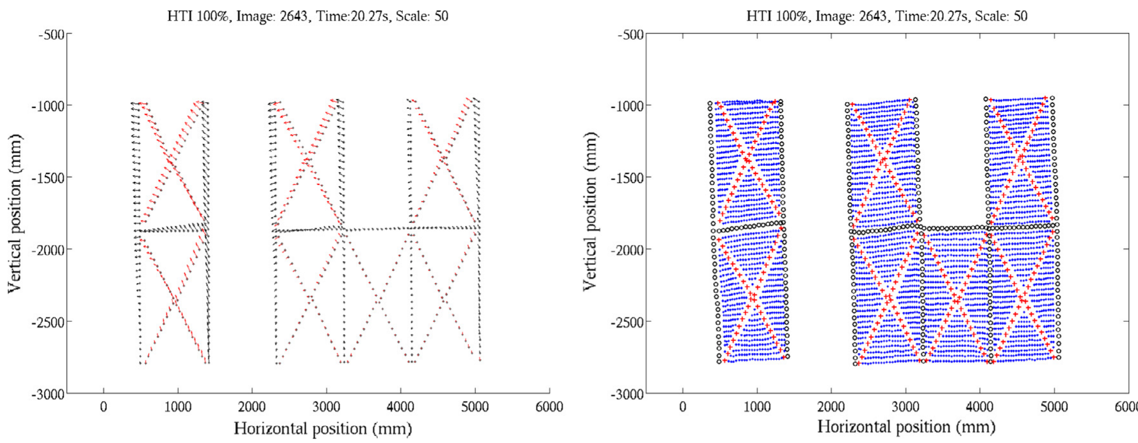

(a) Vector displacement (b) Deformed configuration

Fig. 18. "Haiti 100%" in the negative direction.

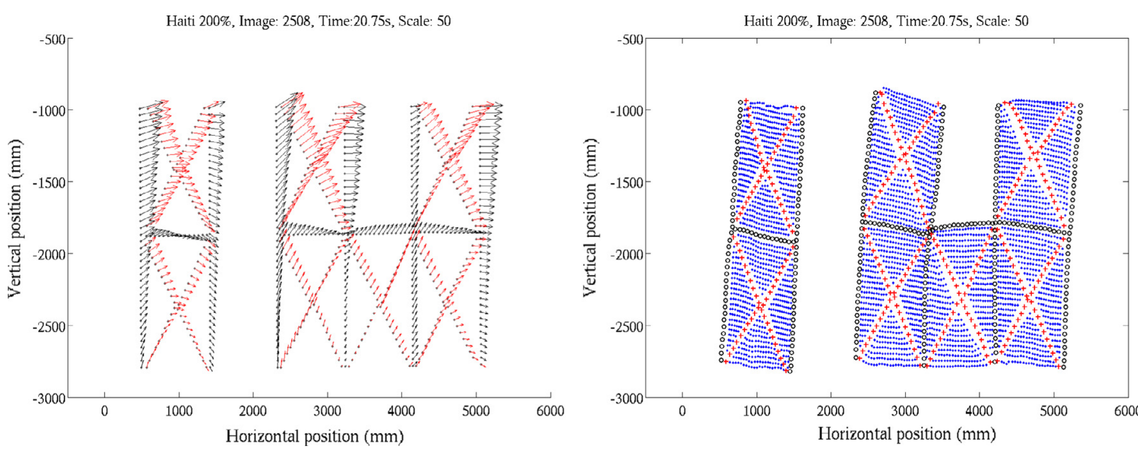

(a) Vector displacement (b) Deformed configuration

Fig. 19. "Haiti 200%" in the positive direction.

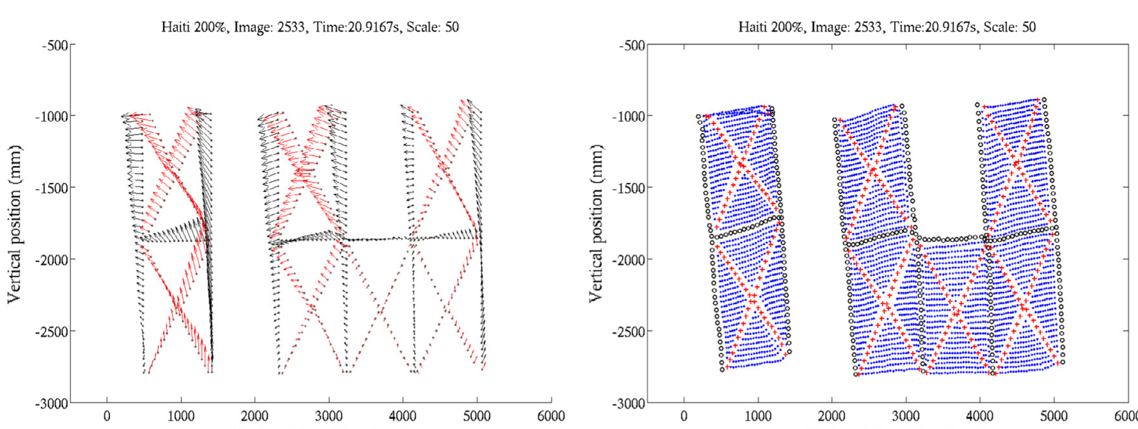

(a) Vector displacement (b) Deformed configuration

Fig. 20. "Haiti 200%" in the negative direction.

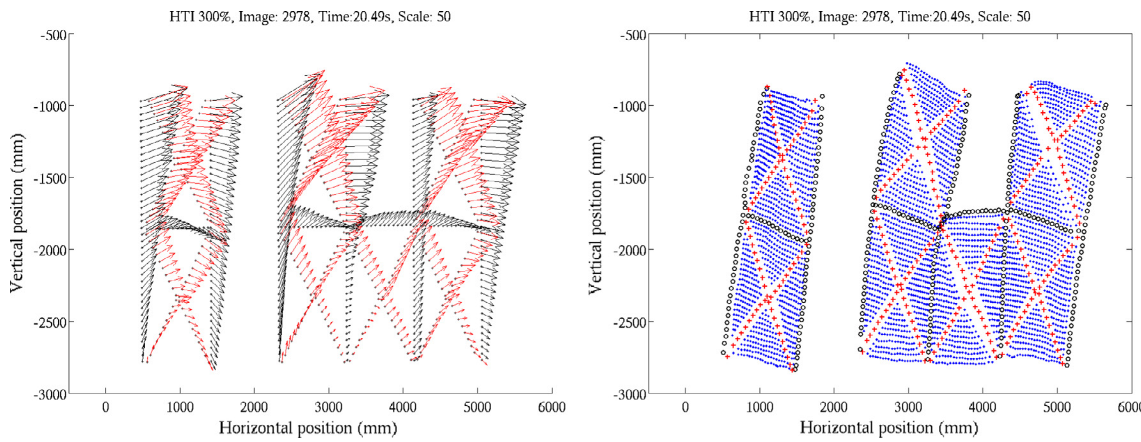

(a) Vector displacement (b) Deformed configuration

Fig. 21. "Haiti 300%" in the positive direction.

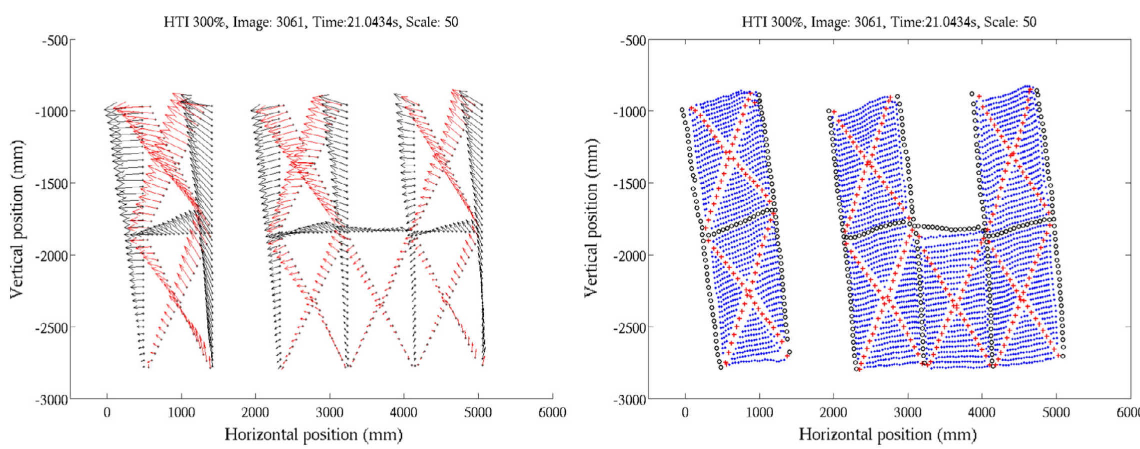

(a) Vector displacement (b) Deformed configuration

Fig. 22. "Haiti 300%" in the negative direction.

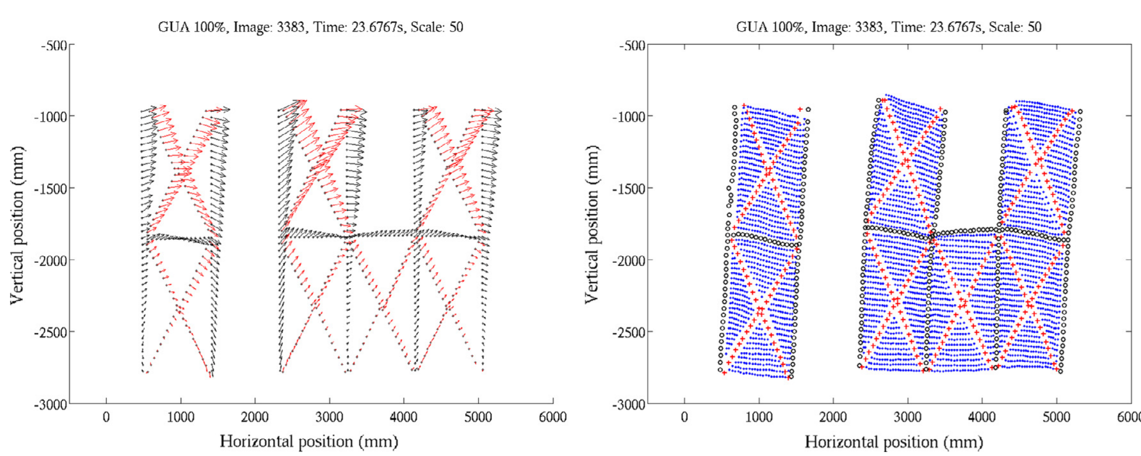

(a) Vector displacement (b) Deformed configuration

Fig. 23. "Guadeloupe 100%" in the positive direction.

The sub-pixel (0.1 of a pixel) is thus essential for the tracking step. The global response for the wall is relevant, and the field of relative displacement is consistent for all pixels, except those that describe the top of the infill material in C1, due to the roof displacement swallow effect.

The displacement field in Figs. 21 and 22 is also relevant and validates the pixel tracking. Only the pixel at the end of the Andrew's crosses has not been correctly tracked. The subset associated with this pixel is slightly too large, and its numerical signature includes some beam pixels that perturb tracking when

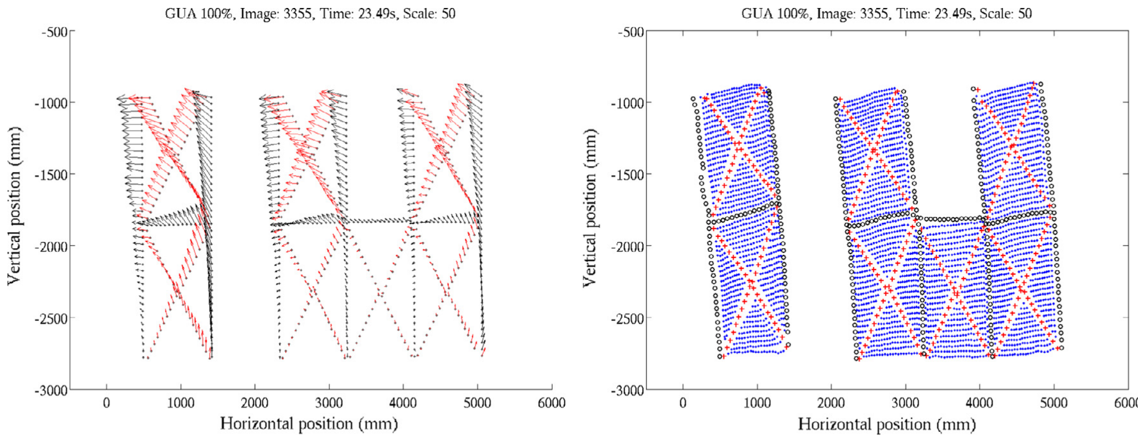

(a) Vector displacement (b) Deformed configuration

Fig. 24. "Guadeloupe 100%" in the negative direction.

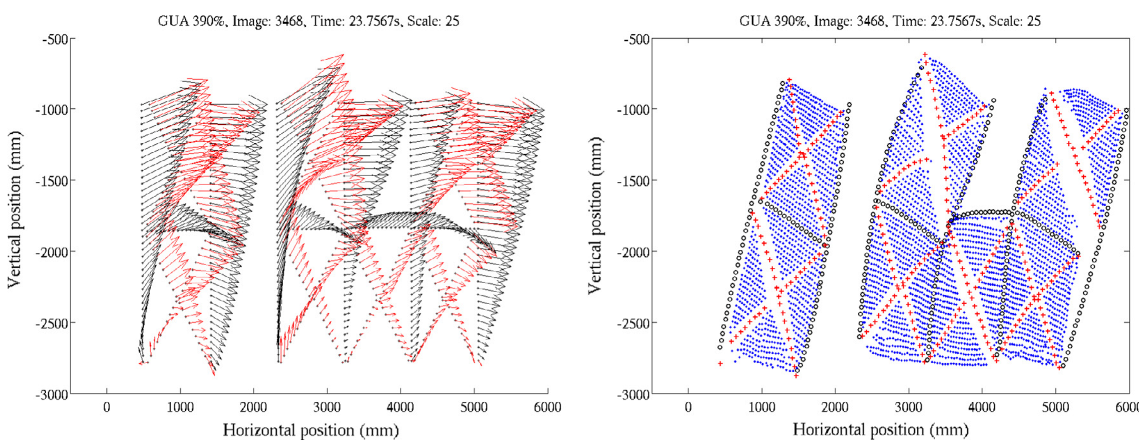

(a) Vector displacement (b) Deformed configuration

Fig. 25. "Guadeloupe 390%" in the positive direction.

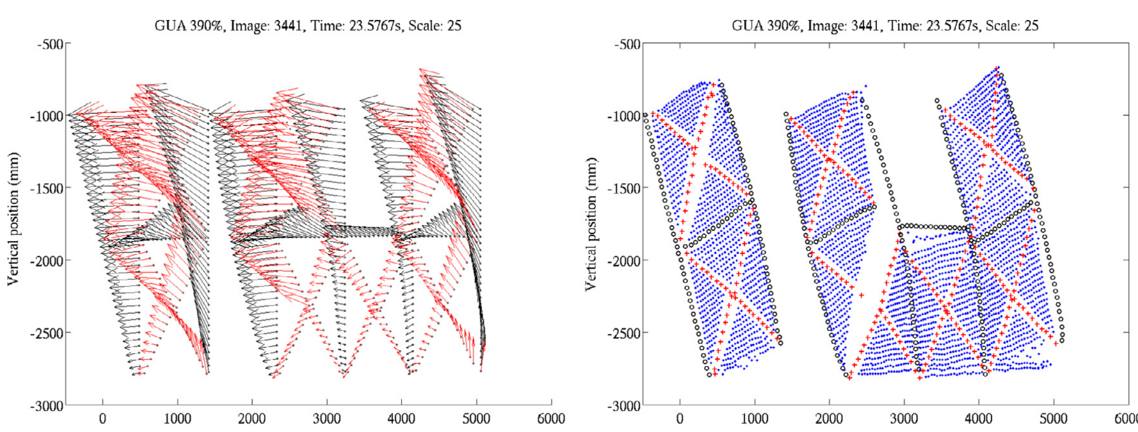

(a) Vector displacement (b) Deformed configuration

Fig. 26. "Guadeloupe 390%" in the negative direction.

the nails are pulled out. This situation applies to 4 pixels of the 3969.

For "Guadeloupe 390%", the displacement field has also been correctly obtained (Figs. 25 and 26) despite the large opening between Andrew's crosses and the infill, which tended to undermine DIC performance.

The relative displacement field has led to partial conclusions. First of all, the structural response is linear for a ground motion equivalent to the January 2010 Haitian earthquake. When increasing the seismic level ("Haiti 200%", "Haiti 300%" and "Guadeloupe 390%"), a nonlinear behavior of the wall is observed. The flexural behavior is clearly depicted in the timber-framed structure in

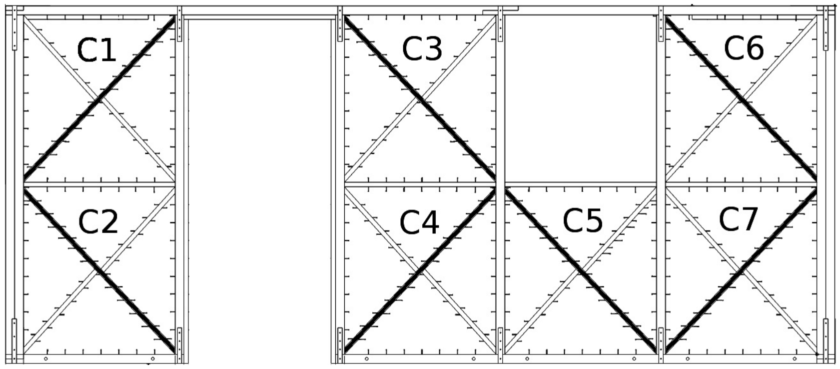

Fig. 27. Continuous diagonals of the Andrew's crosses.

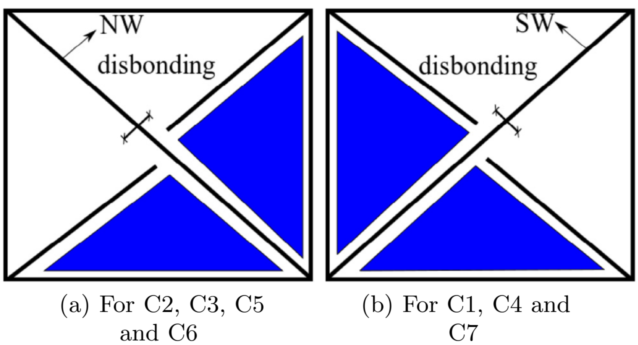

Fig. 28. Definition of the calculated debonding values.

Figs. 19, 20, 21, 22, 25, 26, and this behavior contributes to the energy dissipation.

5.2. Debonding between infill material and Andrew's crosses

In the following discussion, the debonding between infill materials both under and over the continuous diagonals of Andrew's crosses will be addressed. Fig. 27 depicts the continuous diagonals with a black line for the entire wall; they are positioned in one of two ways into cells: with a normal in either the northwest direction or southwest direction (see Fig. 28). It is important to note that 4 cells contain the continuous diagonals in one direction and 3 cells in the other; moreover, for the 3 top cells, 2 continuous diagonals lie in the same direction (C3 and C6). Due to the wall opening (door and window), the wall has an intrinsic asymmetric appearance with continuous diagonals of Andrew's crosses. Fig. 28 presents the debonding calculated for both possibilities of the continuous diagonal direction. The debonding between infill materials and both sides of the continuous diagonal has been calculated by tracking the displacement variations of the two edges of the infill materials, as obtained by the mean value of the pixel displacements. Table 10 summarizes the maximum debonding for each cell and each earthquake. The "+" sign means that the global wall displacement is in the positive direction when debonding occurs, while the "−" sign is used when the global wall direction goes the opposite way. The "Image" number is written for the image which leads to the maximum debonding valor of a cell.

Thanks to this table, it is now possible to analyze the evolution of such debonding, i.e.:

- "Haiti 100%": in accordance with the field displacement presented in Figs. 17 and 18, debonding at this earthquake level is small enough to be insignificant and probably inexistent. Moreover, the calculated debonding values lie in practically the same range of sub-pixel accuracy and, hence, are extremely critical.
- For a positive global wall displacement direction: in all earthquakes, maximum debonding is always obtained in this direction. The debonding in cells C2, C3, C5 and C6 is always predominant. Moreover, debonding is always greater for cell C6 and represents nearly 20% of the maximum wall displacement for all earthquakes, except "Guadeloupe 390%" (at 40%).
- For a negative global wall displacement direction: in all earthquakes except "Guadeloupe 390%", debonding is limited with respect to the other direction, and the maximum is always obtained in cell C1. Outside of C1, cells C4 and C7 (continuous diagonal with a normal in the southwest direction) do not lead to a significant debonding and remain low during the Haiti series. Only for "Guadeloupe 390%" does debonding become significant in cell C4 and over the same C6 maximum debonding range as obtained in the positive direction.

Table 10
Maximum debonding values between infill and continuous diagonals.

Ground motion Cell	Haiti 100% Direction		Haiti 200% Direction		Haiti 300% Direction		Guadeloupe 100% Direction		Guadeloupe 390% Direction	
	+	−	+	−	+	−	+	−	+	−
C1 (mm)	0.16	0.18	0.33	0.80	0.43	**1.5**	0.33	1.08	2.05	**6.6**
C2 (mm)	0.15	0.41	0.63	0.76	**1.49**	0.94	0.72	0.85	**6.34**	3.82
C3 (mm)	0.12	0.08	0.86	0.48	**2.48**	0.58	0.84	0.71	**6.52**	2.74
C4 (mm)	0.13	0.14	0.55	0.68	0.70	0.87	0.57	0.42	1.40	**12.04**
C5 (mm)	0.28	0.09	1.46	0.24	**2.49**	0.42	0.96	0.24	**5.84**	0.5
C6 (mm)	0.67	0.09	1.51	0.25	**2.59**	0.51	1.02	0.41	**14.54**	2.62
C7 (mm)	0.07	0.11	0.20	0.15	0.67	0.28	0.2	0.32	1.93	0.71
Image	2668	2857	2508	2533	2978	3061	3383	3355	3468	3441

Bold values indicate the maximum values of each ground motion.

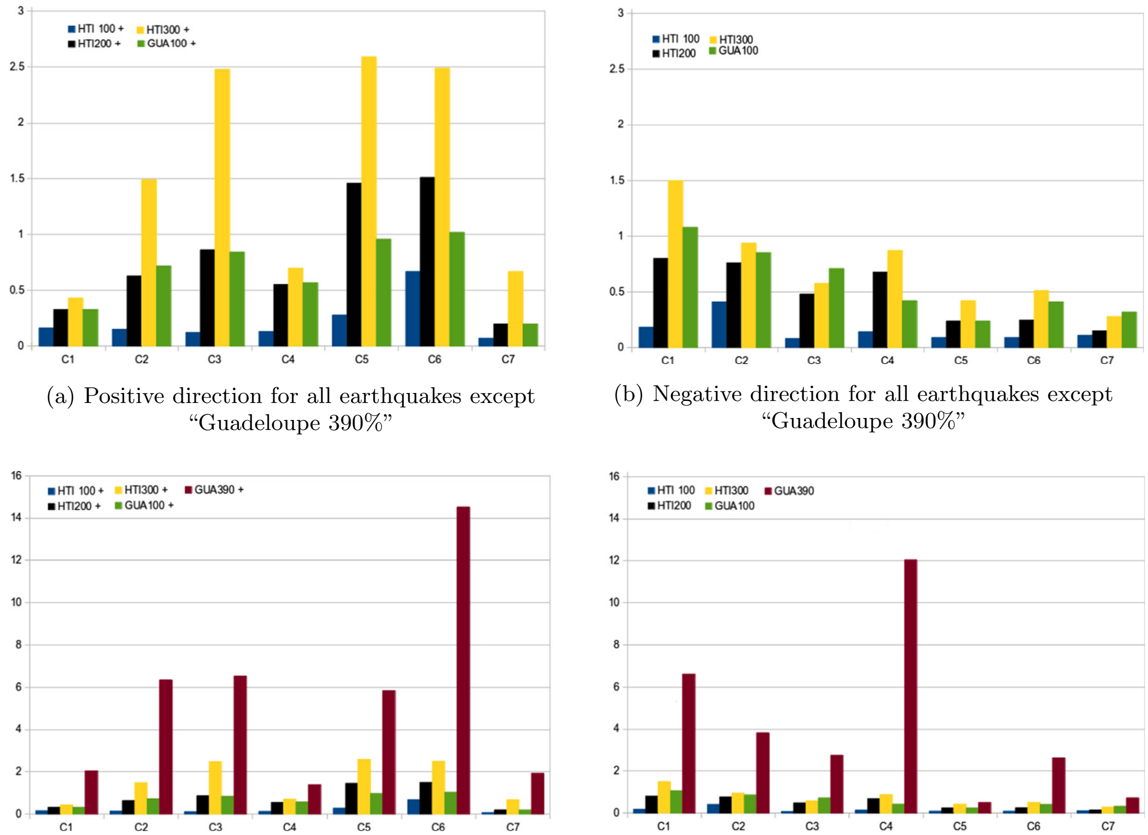

(a) Positive direction for all earthquakes except "Guadeloupe 390%"

(b) Negative direction for all earthquakes except "Guadeloupe 390%"

(c) Positive direction for all earthquakes

(d) Negative direction for all earthquakes

Fig. 29. Maximum gap between discontinuous diagonals.

- The orientation of the continuous diagonals is not in a central vertical symmetry which leads to a debonding always greater in positive direction than in the negative one.
- Zero proportionality: as for maximum displacements, the increase in debonding across earthquake levels is not proportional to the amplification factor of each level. This debonding is likely to account for the largest share of the global wall nonlinearity. The comparison drawn between Fig. 29a and b indicates that this nonlinearity is more pronounced in the positive direction. Only during "Guadeloupe 390%" debonding values are high in both directions (Fig. 29c and d). Nonlinearity is due to accumulated damage that appears significant in both directions of this signal.

5.3. Acceleration and force

Acceleration and, consequently, force are two key observable parameters to evaluate as structural stiffness varies under a seismic loading. Acceleration is calculated using a double derivative of the full-field displacement. This method is indeed relevant since the number of images recorded provides a high level of precision. The excitation period of the wall nears 0.32 s for each earthquake, and then 48 images are available despite the vibration of each point in the wall. For each pixel and at a given time t, a second-order polynomial has been chosen to fit the displacement curvature defined by 7 points (including 3 after and 3 before t). A first derivative is taken and a new second-order polynomial is found to fit the speed curvature also defined by 7 points. At this point, a second derivative corresponding to the acceleration is taken. Next, the horizontal acceleration of the shake table obtained with DIC is compared to the horizontal acceleration recorded by an accelerometer on the shake table. Fig. 30 shows that acceleration has been properly determined with DIC: the curvature of both accelerations is similar. Based on the frequency domain responses obtained by a Fast Fourier Transform (FFT), the Fig. 31 confirms the same assumption. This is a very powerful outcome since the acceleration could be calculated everywhere on the wall and during data post-processing. It is also possible to find the acceleration in both directions for each pixel tracked.

5.4. Global shear wall force vs post right displacement

Fig. 32 exhibits the diagram of the wall force function of the top right wall displacement. The shear used as a basis has been computed by summing the inertial forces of all 7 cells from the horizontal acceleration obtained by DIC. For each elementary cell with infill, cell weight has been evaluated at 150 kg.

The hysteretic responses of the test structure, as calculated with DIC during the Haitian and Guadeloupean series, highlight the trend in case of an overall nonlinear behavior. For "Haiti 100%", the overall behavior is linear, thus highlighting that the structure is highly resistant to a ground motion equivalent to Haiti's January 2010 earthquake. The nonlinearity and dissipated energy increase as stiffness decreases (Fig. 32) after each "Haiti 200%" and "Haiti 300%" signal, which reveals structural damage. Following repairs and during "Guadeloupe 100%", overall behavior is definitively nonlinear and effective stiffness has slightly decreased relative to "Haiti 300%". This finding may be explained by a lack of impact from the overall shear wall repair: irreparable damage in the infill material; and interface degradation after debonding, as discussed above. On the other hand, repairs relative to the global response of the entire house are indeed relevant (Table 11): roof structure

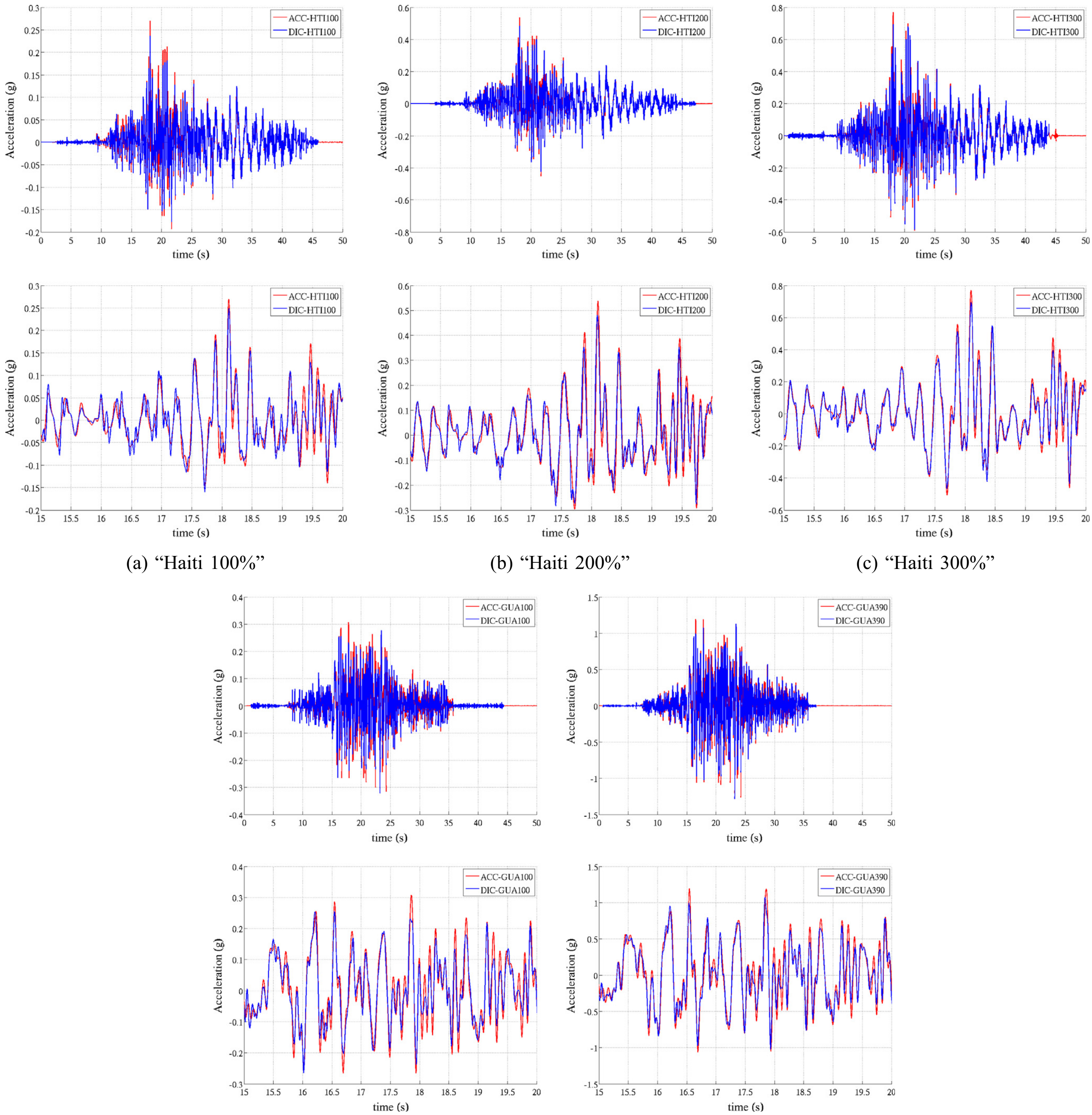

(a) "Haiti 100%" (b) "Haiti 200%" (c) "Haiti 300%"

(d) "Guadeloupe 100%" (e) "Guadeloupe 390%"

Fig. 30. Acceleration – comparison between DIC and accelerometer for the shake table (all signals and close-ups near the peak).

bracings exert a strong influence on the structural behavior of the transverse wall.

The overall behavior observed during "Guadeloupe 390%" reflects a typical hysteresis curve with good seismic structural dissipation capacity (as regards the considerable level of seismic ground motion). More specifically, the wall's ability to withstand large displacements without reaching failure is highlighted. Moreover the shear wall presents even ability to develop resistant capacity as the shear capacity developed for this seismic input is higher than the one observed during "Haiti 300%".

Figs. 33 and 34 depict the hysteretic responses of each cell vs. its average displacement for both "Haiti 300%" and "Guadeloupe 390%". For the two earthquake signals, energy dissipation is predominant in cells C1, C3 and C6, which are the top ones. Even for "Guadeloupe 390%", dissipation in the bottom cells is not caught in this representation. Consequently, no direct correlation exists between debonding (significant in C4 with "Guadeloupe 390%") and the hysteretic response of a cell.

6. Discussions

As highlighted in Figs. 17 and 18, the structural response obtained during "Haiti 100%" is linear. The structure resisted well to a ground motion equivalent to Haiti's January 2010 earthquake.

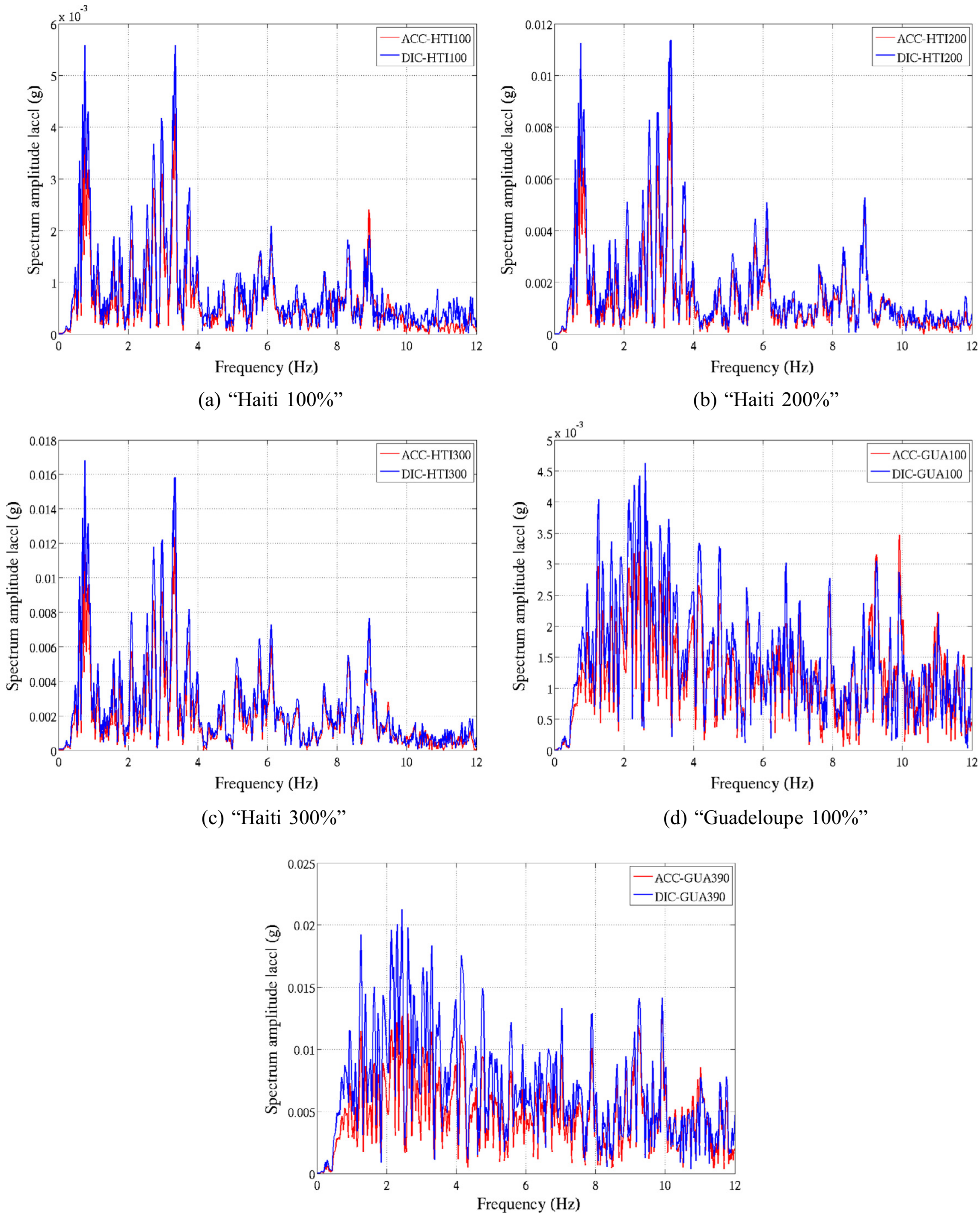

(a) "Haiti 100%" (b) "Haiti 200%"

(c) "Haiti 300%" (d) "Guadeloupe 100%"

(e) "Guadeloupe 390%"

Fig. 31. FFT – comparison between DIC and accelerometer results for the shake table.

No damage could be observed, a finding that provided direct proof of the seismic-resistant behavior of timber-framed structures containing infill.

Five earthquake signals with high energies were introduced to perform the shake table tests on the same building. No damage could be observed on the shear walls, and only two infill triangles were pulled out onto one transverse wall. The building definitively features a seismic-resistant behavior since it is capable of preventing injury to dwelling occupants (i.e. no mortal risk).

Thanks to a DIC analysis, this article has highlighted the ductility of the building, which is thus able to exhibit large-scale displacements and a high energy dissipation capacity. More specifically, the DIC study has yielded critical information about: the flexibility of a timber-framed structure, and the debonding between continuous diagonals of the Andrew's crosses and infill. These are the key issues raised herein and will be further discussed below.

The continuous diagonals allow decoupling the behavior of a cell into two distinct triangles. For a high-energy ground motion,

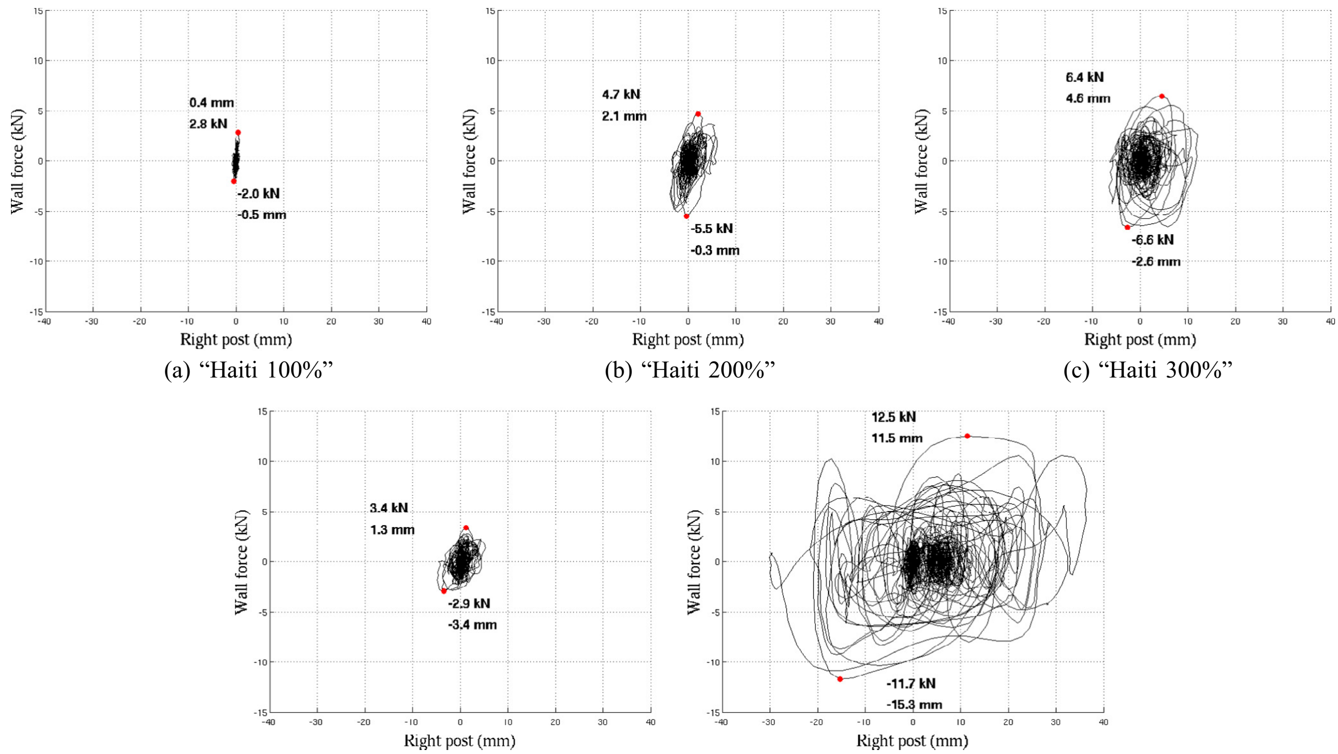

(a) "Haiti 100%" (b) "Haiti 200%" (c) "Haiti 300%" (d) "Guadeloupe 100%" (e) "Guadeloupe 390%"

Fig. 32. Global shear wall force vs. right post displacement.

Table 11
Effective stiffness values.

Earthquake	Haiti 100%	Haiti 200%	Haiti 300%	Guadeloupe 100%	Guadeloupe 390%
Shear wall global hysteretic response (kN/mm)	5.31	4.25	1.82	1.34	0.90

the triangles below the continuous diagonal isolate themselves from the upper triangle, which then follows its course of movement without driving the lower triangle. This debonding serves to dissipate energy with no infill disaggregation. Only the bond between diagonal and infill is loaded, before returning to its initial state upon loading. This safety issue is raised because discontinuous diagonals are unable to contribute in tension: the nail connection provides an opportunity to pull out and release the two triangles on each side of the continuous diagonal. For continuous diagonals, the nail connection is also a pull-out type with tension, which leads to a disconnection between these diagonals and the vertical posts. The connection of Andrew's crosses then becomes particularly relevant given their extreme simplicity and effectiveness in improving ductility and seismic resistance of the structure. The more rigid connection, such as a lap joint, used in the "Pombalino" wall (see [17,26]) therefore seems to be less relevant.

The discontinuous diagonals in the shear wall only exert an impact when in compression. The infill however is already quite strong in compression, hence the impact of these discontinuous diagonals remains questionable. Yet one purpose of the Andrew's crosses is to divide the rectangular cells into 4 triangles in order to prevent cell infill materials from collapsing all at once. As mentioned in Section 3, no infill material collapse occurred for the shear wall, although infill materials of two triangles did fall with the "Guadeloupe 390%" transverse wall (Fig. 12d). An investigation would be needed to understand what would have happened without the discontinuous diagonals. "Guadeloupe 390%" represents a high-energy earthquake signal, and it does not seem reasonable to use it in structural design since no infill material has fallen for the other 4 signals. A second purpose of discontinuous diagonals consists of helping fill cells during construction. Nevertheless, this still induces a global construction cost. In the context of Haitian reconstruction and according to the prevailing world view, timber material savings is an incentive behind this kind of construction. The main conclusion of these DIC analyses is their non-necessity in future projects.

The second key issue would be the importance of the continuous diagonal design. To ensure a dissipative wall behavior in both directions, a central vertical and axial symmetry must be derived to the greatest extent possible. In the case studied herein, such symmetry cannot be obtained due to the opening, hence the southern direction is less dissipative than the north (i.e. debonding is always greater in the positive direction than in the negative one), which is probably correlated with observed damage on the transverse wall: for "Guadeloupe 390%", two triangles fall on the southern transverse wall whereas no damage is observed on the northern out-of-plane wall.

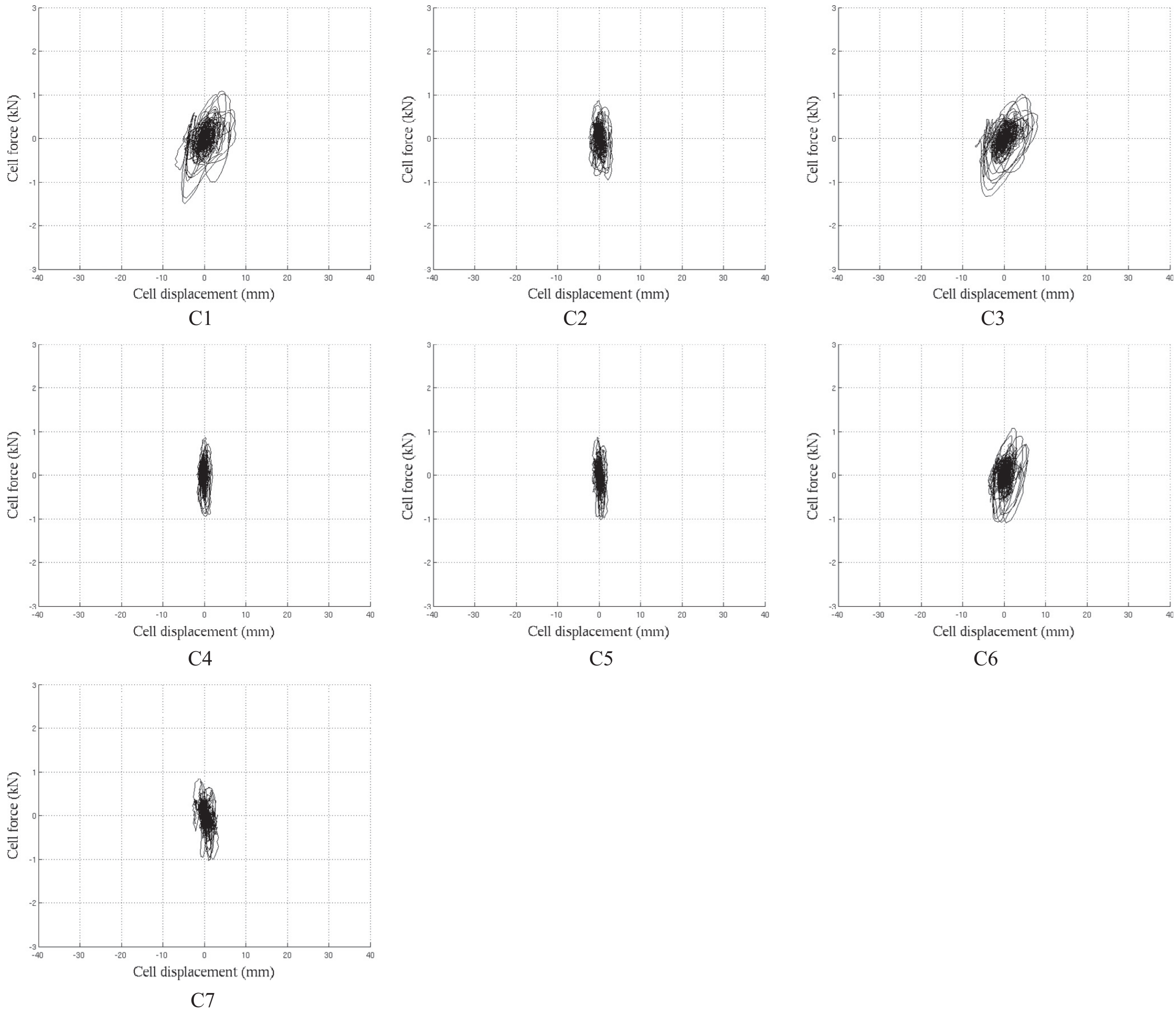

Fig. 33. Shear wall force in the cell vs. cell displacement for “Haiti 300%”.

7. Conclusion

This paper has presented a field displacement measurement method with use of a high-speed camera. The innovation herein is to explain and prove the feasibility of this method for a large sample displaying the actual dimensions of a house wall (9.3 m^2) and under a seismic loading applied by a shake table. Following a technical description of the system’s components (camera and lighting), emphasis was placed on the painted speckle pattern and its connection to the subset chosen for pixel tracking with the DIC software.

To validate this DIC analysis, a comparison was drawn with the displacement recorded by LVDT. The difference between the two measurements was less than 5%. In another part of the paper, the acceleration was found in every pixel tracked using a second derivative of the displacement field. A comparison could also be drawn with an accelerometer on the shake table. For certain ground motion signals, the difference in peak values was significant, yet the time acceleration curve remained in good agreement.

One of the main advantages of field measurements relative to local measurements, as obtained with LVDT, DWDS and an accelerometer, was also highlighted: the possibility of generating information at the level of each pixel, which enables selecting them individually in a post-process analysis.

The global response of the shear wall was analyzed through results of the field displacement measured on 3969 pixels to describe each component (timber-framed structure plus infill). These databases served to plot a 2D view of the global deformed configuration for 5 ground motion signals. The structural response is linear for a ground motion equivalent to Haiti’s January 2010 earthquake, which provides scientific proof of its seismic-resistant quality and validates the relevance of this type of building in Haiti’s reconstruction project. At an increased seismic level (“Haiti 200%” and “Haiti 300%”), nonlinear wall behavior is observed. Flexural behavior, which helps dissipate energy, has been identified in the timber-framed structure.

This view of the deformed configuration has revealed an opening between the connection of the Andrew’s cross continuous diagonal and the infill. Special attention was paid to quantifying this debonding. Like for displacements, debonding was not proportional to the increased amplitude factor scaling of earthquake signals. Asymmetric behavior was also exhibited and explained by the

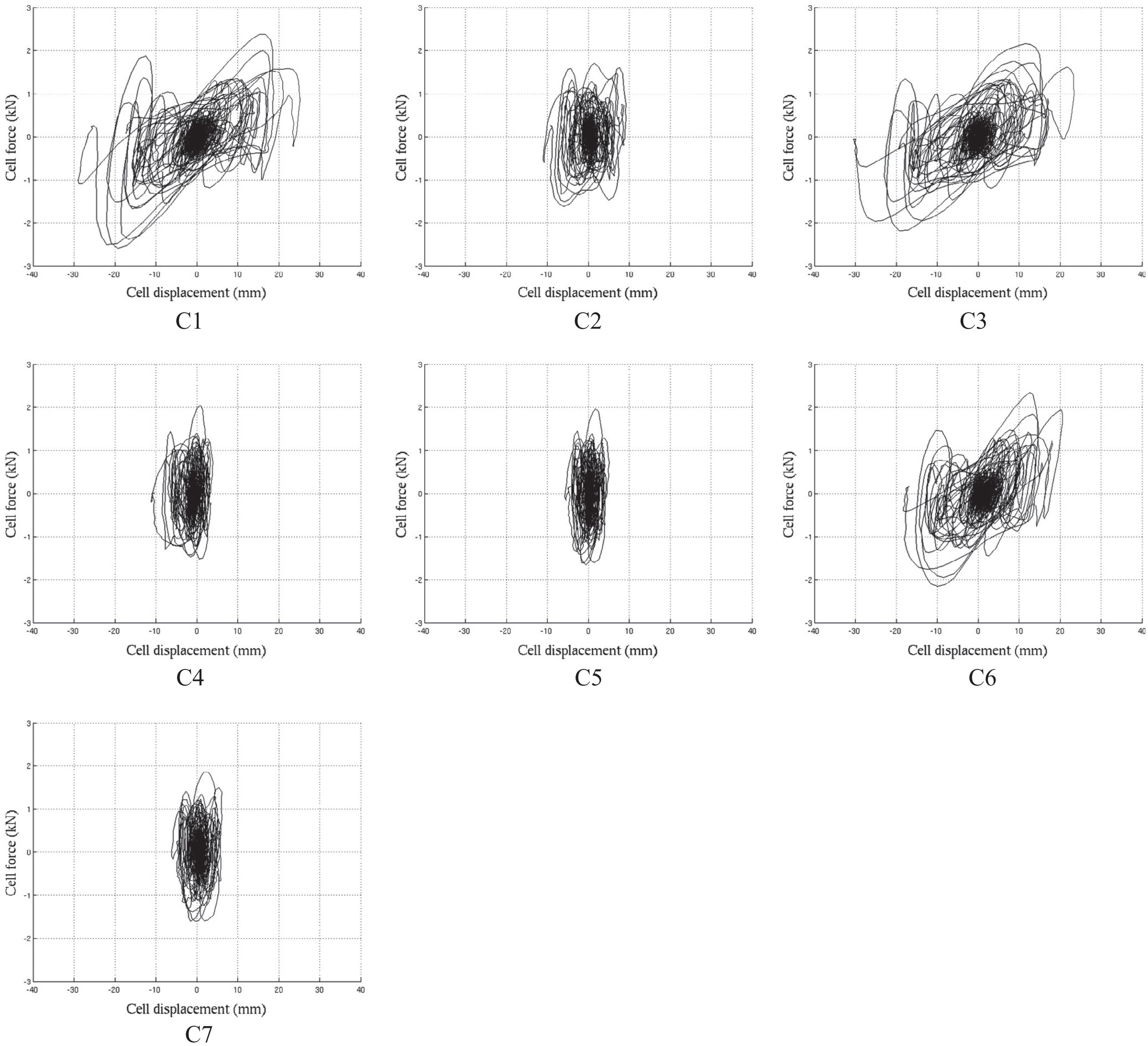

Fig. 34. Shear wall force in the cell vs. cell displacement for ''Guadeloupe 390%''.

continuous diagonal position. Debonding between continuous diagonal and infill was key to understanding the seismic-resistant behavior of this type of building. Such opening interfaces allowed for large wall displacements, accompanied by energy dissipation and without any infill disaggregation; they played a role similar to that of a fuse. Moreover, by calculating the acceleration in each pixel tracked, the global wall force could be obtained. The hysteretic response of the shear wall was plotted for each ground motion; a similar evolution for the house and shear wall global hysteretic response was found with the seismic signals, meaning that damage in the shear wall is representative of global house damage. A DIC analysis yielded the global force on the shear wall, which also provided a better understanding of the behavior of this kind of structure.

The final section was devoted to the impact of continuous and discontinuous diagonals with respect to dissipation energy for high-energy ground motion. The choice of bracing proved relevant in providing ductility and strength at these loading levels. The article concluded that timber savings appear to be possible since the impact of discontinuous diagonals is subject to debate. A recommendation was also forwarded regarding the position of bracing for future (re)construction projects.

Field displacement measurements provide a direct proof of the seismic-resistant behavior of a filled timber-framed structure.

Acknowledgements

The authors would like to thank and acknowledge the French National Research Agency (ANR) for its support of the ''ReparH'' project, under reference code ANR-10-HAI-003 (as coordinated by CRAterre in collaboration with UJF-3SR, the AE&CC Research Unit of ENSAG and the Haitian NGO GADRU), along with all participating associations of the PADED platform and local partners for their involvement and contributions to this endeavor. This work has also been supported by a public grant overseen by the French ANR as part of the ''Investissements d'Avenir'' program (reference:

ANR-10-LABX-0083). The authors extend their gratitude to the multidisciplinary building team, composed of: Nicolas Beghin, Christian Belinga Nko'o, Fabrizio Boghi, Sophie Claude, Cécilia Doveri, Frédérique Jonnard, Jasim Taher Mohammad, Noro Ravoavahy, Yannick Sieffert, Juan Trabanino, and Florent Vieux-Champagne. Thanks are also addressed to FCBA technical staff for the tests they conducted, as well as to Simon Pla and François Bonnel (IRIS) for their valuable assistance throughout the experimental program.

References

[1] Aktas YD, Akyüz U, Türer A, Erdil B, Sahin Güçhan N. Seismic resistance evaluation of traditional Ottoman timber-frame himis houses: frame loadings and material tests. Earthquake Spectra 2014;30(4):1711–32.

[2] Ali Q, Schacher T, Ashraf M, Alam B, Naeem A, Ahmad N, et al. In-plane behavior of full scale Dhajji Walls (Wooden Braced with Stone Infill) under quasi static loading. Earthquake Spectra 2012;28(3):835–58.

[3] Ceccotti A, Faccio P, Nart M, Simeone P. Seismic behavior of wood framed buildings in Cadore mountain regioni – Italy. In: 13th World conference on earthquake engineering. p. 14.

[4] Combe G, Richefeu V. Tracker: a particule image tracking (PIT) technique dedicated to nonsmooth motions involved in granular packings. In: Powders and grains 2013: proceedings of the 7th international conference on michromechanics of granular media. vol. 1542(1). AIP Conf. Proc; 2013. p. 461–4.

[5] Doğangün A. Performance of reinforced concrete buildings during the May 1, 2003 bingöl earthquake in Turkey. Eng Struct 2004;26:841–56.

[6] Doğangün A, Tuluk O-I, Livaoğlu R, Acar R. Traditional wooden buildings and their damages during earthquakes in Turkey. Eng Fail Anal 2006;13:981–96.

[7] Dutu A, Sakata H, Yamazaki Y. Experimental study on timber-framed masonry structures. Hist Earthquake–Resistant Timber Frames Mediterr Area 2014:67–81.

[8] Goodall C. Peak stuff – did the uk reach a maximum use of material resources in the early part of the last decade? Carbon commentary 2011; 2011. <http://www.carboncommentary.com/wp-content/uploads/2011/10/Peak_Stuff_17.10.11.pdf> [accessed 15 October 2014].

[9] Hua T, Xie H, Wang S, Zhenxing H, Chen P, Zhang Q. Evaluation of the quality of a speckle pattern in the digital image correlation method by mean subset fluctuation. Optics Lasers Eng 2011;43:9–13.

[10] Hyoung-Suk C, Jin-Hwan C, Sang-Hyo K, Jin-Hee A. Structural dynamic displacement vision system using digital image processing. NDT&E Int 2011;44:597–608.

[11] Khasreen MM, Banfill PFG, Menzies GF. Life-cycle assessment and the environmental impact of buildings: a review. Sustainability 2009;1:674–701.

[12] Langenbach R. Preventing pancake collapses: lessons from earthquake-resistant traditional construction for modern buildings of reinforced concrete. In: International Disaster Reduction Conference (IRDC), Davos, Switzerland; 2006. p. 44.

[13] Langenbach R. From 'opus craticium' to the 'chicago frame': earthquake resistant traditional construction. Int J Archit Heritage 2007;1:29–59. Taylor & Francis.

[14] Langenbach R. Learning from the past to protect the future: armature crosswalls. Eng Struct 2008;30:2096–100.

[15] Lecompte D, Smits A, Bossuyt S, Sol H, Vantomne D, Van Hemelrijck D, et al. Quality assessment of speckle patterns for digital image correlation. Optics Lasers Eng 2006;44(11):1–17.

[16] Makarios T, Fosthenous M. Seismic response of traditional buildings of Lefkas Island, Greece. Eng Struct 2006;28(2):264–78.

[17] Meireles H, Bento R, Cattari S, Lagomarsino S. A hysteretic model for frontal walls in Pombalino buildings. Bull Earthquake Eng 2012;10(5):1481–502.

[18] Pan B. Recent progress in digital image correlation. Exp Mech 2011;51(7):1223–35. Available from: <http://dx.doi.org/10.1007/s11340-010-9418-3>.

[19] Pan B, Qian K, Xie H, Asundi A. Two-dimensional digital image correlation for in-plane displacement and strain measurement: a review. Meas Sci Technol 2009;20:1132–45.

[20] Poletti E, Vasconcelos G. Seismic behaviour of traditional timber frame walls: experimental results on unreinforced walls. Bull Earthquake Eng 2015;13(3):885–916.

[21] Ribeiro D, Calçada R, Ferreira J, Martins T. Non-contact measurement of dynamic displacement of railways bridges using an advanced video-based system. Eng Struct 2014;75:164–80.

[22] Richefeu V, Combe G, Viggiani G. An experimental assessment of displacement fluctuations in a 2d granular material subjected to shear. Géotechnique Lett 2012;2:113–8.

[23] Shih M-H, Sung W-P. Developing dynamic digital image techniques with continuous parameters to detect structural damage. Hindawi Publishing Corporation; 2013. p. 1-7.

[24] Sieffert Y, Huygen J-M, Daudon D. Sustainable construction with repurposed materials in the context of a civil engineering earchitecture collaboration. J Cleaner Prod 2014;67:125–38.

[25] van de Lindt J, Pei S, Pryor SE, Shimizu H, Isoda H. Experimental seismic response of a full-scale six-story light-frame wood building. J Struct Eng 2010;136(10):1262–72.

[26] Vasconcelos G, Poletti E, Salavessa E, Jesus AM, Lourenço PB, Preecha P. In-plane shear behavior of traditional timber walls. Eng Struct 2013;56:1028–48.

[27] Vieux-Champagne F, Grange S, Sieffert Y, Garcia P, Faye C, Duccini J-C, et al. Numerical analysis of timber-frame structures with infill under seismic loading. World Conference on Timber Engineering (WCTE) 2014, Quebec City, Canada, August 10-14; 2014.

[28] Vieux-Champagne F, Sieffert Y, Grange S, Polastri A, Ceccotti A, Daudeville L. Experimental analysis of seismic resistance of timber-framed structures with stones and earth infill. Eng Struct 2014;69:102–15.